JOURNAL OF GEOPHYSICAL RESEARCH, VOL. 95, NO. C7, PAGES 11,461–11,482, JULY 15, 1990

Tropical Data Assimilation Experiments With Simulated Data: The Impact of the Tropical Ocean and Global Atmosphere Thermal Array for the Ocean

ROBERT N. MILLER

College of Oceanography, Oregon State University, Corvallis

A series of observing system simulation experiments (OSSE) is performed on a simulated data set which was designed to mimic the wind-forced response of the tropical Pacific ocean. This data set was constructed by adding random perturbations to the FSU monthly mean pseudostress anomaly data. These perturbed pseudostress anomaly fields were used to drive a simple linear model whose output was sampled to form synthetic observations. The statistics of the perturbations are given by estimates of the errors in the pseudostress data calculated in an earlier study. OSSE are performed using simulated sea level height data from island tide gauge stations and from selected TOGA-TAO (Tropical Ocean and Global Atmosphere Thermal Array for the Ocean) mooring sites. Data from the TOGA-TAO moorings are assumed, in one experiment, to consist of sea level height data, identical to that from tide gauges. In a further experiment, mooring data consist of amplitudes of the first two vertical modes. Errors in the OSSE are seen to be comparable to errors obtained in comparison to real data where such comparisons are available. Assimilation of data at six island stations results in noticeable, but not dramatic improvement in the analysis, as was noted in an earlier study with actual observations. OSSE using simulated mooring data showed accuracy in the sea level height field comparable to that of the instruments across much of the basin. Inclusion of the separate baroclinic modes resulted in negligible improvement. Simulated fields of 20° isotherm depth anomaly were also produced. Results were similar to the sea level height results. As in the simulation of sea level height, inclusion of the separate baroclinic modes resulted in negligible improvement.

1. INTRODUCTION

In an earlier study ([*Miller and Cane*, 1989], hereinafter referred to as MC), the efficiency of assimilating data at six island stations was investigated and error bounds were determined. Those results showed that data assimilation at only six island locations in the tropical Pacific resulted in enriched structure of the sea level height field, most interestingly in places removed from the island stations where data were collected for assimilation. Because of the lack of data in the tropical Pacific, only partial verification was possible. One way to investigate the question of whether the structure introduced by the assimilation process is really there is to produce a simulated data set by forcing the model with winds to which a random perturbation has been added, using the output from that model run as if that were the true state of the ocean, and sampling that state to obtain data for assimilation into model runs forced by the unperturbed winds. Comparisons can then be made between the results so obtained and the reference data set derived from the perturbed winds.

In MC, actual sea level observations were used for assimilation and verification. In this study, a simulated data set is generated and observing system simulation experiments (OSSE) are performed. The results from assimilation of synthetic data at six island stations corresponding to those used in MC are presented. The improvement of the model analysis by assimilation of sea level height data at six stations was quantitatively small, as one would expect from such a sparse observational network. The analysis is particularly suspect in the eastern part of the basin west of the Galapagos where there are no island tide gauge stations along the equator. Since the six island stations do not provide enough data for reliable basin-wide analyses, it is natural to ask how much is to be gained by including other data sets. One practical candidate is the TOGA–TAO array (TOGA Thermal Array for the Ocean; *Hayes* [1989]). This array of moored instruments occupies several locations in this data void region. Data from the 500 m thermistor chains on these moorings can be used to calculate dynamic height. These temperature profile data are now available in real time via satellite.

A series of OSSE with similar intent was performed with a very similar physical model by *Long and Thacker* [1989]. That study focused on the impact of satellite altimeter data upon four-dimensional model-aided analysis of the tropical ocean. Even with much more dense (simulated) observational networks than the ones investigated here, and with model experiments of considerably shorter duration, they found that surface observations alone were not sufficient to reconstruct the full state of the tropical ocean. Their aim, however, was an ambitious one: they wished to reconstruct the details of the vertical structure of the ocean, so they calculated the amplitudes of a large number of vertical modes. In the experiments reported here, only two vertical mode amplitudes are calculated. While the details of the vertical structure are poorly resolved by this approximation, integrated quantities such as dynamic height are well represented. At this level of approximation,

Paper number 90JC00810.
0148-0227/90/90JC-00810$05.00

the results of Long and Thacker are consistent with those presented here: surface observations are enough to determine the horizontal structure of the amplitudes of the two lowest baroclinic modes.

In MC, only sea level height anomaly fields were calculated. In these simulation experiments, an attempt is made to model the anomaly in the depth of the 20° isotherm as well.

Section 2 contains a review of the model and the Kalman filter. The construction of the simulated data set is described in detail in section 3. Section 4 contains a discussion of the manner in which the observations were simulated. Section 5 contains detailed descriptions of the OSSE. Section 6 contains discussion and summary.

2. Review of the Model and the Kalman Filter

In this study as in MC, the physical model is a simple linear wave model driven by the FSU monthly wind pseudostress analysis, produced by Florida State University, based on surface data [*Goldenberg and O'Brien*, 1981]. The analyzed wind fields are applied in the form of monthly mean pseudostress anomalies from the climatological average for each month. All quantities thus appear in the form of deviations from the climatological monthly mean. Island tide gauge data and simulated mooring data are assimilated using the Kalman filter. The model and the Kalman filter are described very briefly here. Details can be found in MC.

The physical model used here, the linearized equations of motion on an equatorial beta plane, has been described many places. As described by *Cane* [1984], the motion is decomposed into vertical modes. The amplitude of each vertical mode satisfies the linearized shallow water equations on the beta plane, subject to long wave approximations. The motion in each vertical mode is further decomposed into a superposition of Kelvin and Rossby waves. The amplitudes of these waves are governed by simple advection equations. Two vertical modes are retained, following *Cane's* [1984] study which showed that these two modes dominate the sea level response during El Niño. Five meridional Rossby modes are retained for each vertical mode in the present calculations. Sensitivity studies reported in MC showed that retaining as many as nine Rossby modes produced no discernible improvement in the results.

Linearized shallow water models on the equatorial beta plane such as the one used here have been widely used in the modeling of the response of the tropical ocean to wind forcing; see, e.g., *Cane* [1984 and references therein]; see also *Cane and Busalacchi* [1987]. Questions about the suitability of homogeneous models linearized about a uniform resting background remain. Some detailed reports of investigations of the consequences of some of the specific assumptions underlying this model have appeared. *Busalacchi and Cane* [1988] considered the consequences of the assumption of spatial homogeneity of stratification. They found that relaxation of that assumption would not account for the errors in earlier homogeneous simulations. *McPhaden et al.* [1986] examined some of the consequences of relaxing the assumption of a uniform resting state. They found little effect on the lowest baroclinic modes.

While the limits of applicability of linear models have yet to be established, they are known to be effective at the simulation of integrated quantities such as sea level height. In restricting consideration to linear models, we sacrifice proper treatment of the amplification of long waves by barotropic instability of the mean state (see, e.g., *Weisberg* [1987 and references therein]). It is possible that these waves make little net contribution to annual or interannual sea level signal, since the fastest growing modes have periods of several weeks, and are thus at the threshold of the temporal resolution of this and other commonly used linear models.

Inclusion of these instability waves in this system would involve a considerable increase in complexity, both in the dynamical model and the statistical error model, since the contribution of these waves to the dynamic topography of the tropical Pacific is inhomogeneous in space and subject to significant seasonal variation. It is not clear that the available data justify the use of such a complex model for the purpose of array evaluation by OSSE. *Hayes et al.* [1989] constructed a data assimilation system consisting of a form of optimal interpolation and a fully nonlinear model, and found that the details of the instability waves were not accurately reproduced.

Incorporation of features that involve an inhomogeneous mean state would add considerably to the complexity of the model, and the rewards to be gained in this context from the additional labor are doubtful. In order to relax the assumption of a homogeneous mean state, the prospective model designer would have to grapple with the fact that the mean state is itself poorly known.

Though some doubts remain, existing studies do not give us reason to believe that the gross physical simplicity of the homogeneous linear models leads to biases or to the development of qualitatively inaccurate maps of sea level height or other integrated quantities. The qualitative skill of linear models is well established. The contribution of nonlinear effects in a detailed error budget is obscured by uncertainty in the forcing fields.

The data assimilation method used here is the Kalman filter, which has been described in detail in many places (see, e.g., *Gelb* [1974]). The Kalman filter was first formulated in the meteorological context by Ghil (see, e.g., *Ghil et al.* [1981]) and later applied to a prototype problem in numerical ocean modeling by *Miller* [1986]. A brief description follows.

The Kalman filter is most conveniently described through a state space approach. For each of the two vertical modes, five meridional Rossby mode amplitudes and a Kelvin wave amplitude are calculated at each longitude. The model domain extends from 125°E to 80°W in 5° intervals. Thus there are 12 values at each of the 32 gridpoints in the model domain for a total of 384 values at each time. These values are the components of the state vector $\mathbf{w}$, which completely specifies the model. A numerical scheme for this system, from this viewpoint, is a method which, given a state vector and a wind field, can predict the state vector at the next time step, 10 days hence in this case.

Within this framework, we may write the numerical model as

$$\mathbf{w}_{k+1}^{f} = \mathbf{L}\mathbf{w}_{k}^{a} + \boldsymbol{\tau}_{k}$$

where the subscripts denote time step, superscript "f" denotes "forecast" and superscript "a" denotes "analysis," the best available estimate of the state vector at time t_k.

The vector $\boldsymbol{\tau}$ is the forcing. The matrix $\mathbf{L}$ represents the numerical scheme for the evolution of the amplitudes of the Kelvin and Rossby waves in each baroclinic mode.

The model system is assumed to differ from the true system by random noise, i.e., the underlying dynamics obey

$$\mathbf{w}_{k+1}^t = \mathbf{L}\mathbf{w}_k^t + \boldsymbol{\tau}_k + \mathbf{b}_k$$

where the quantities with the superscript "t" represent the true system. $\mathbf{b}_k$ is a random variable uncorrelated from time step to time step:

$$\left\langle \mathbf{b}_j \mathbf{b}_k^T \right\rangle = \mathbf{Q}_k \delta_{jk}$$

where each $\mathbf{Q}_k$ is a positive semidefinite matrix which we shall refer to as the "system noise covariance." The superscript "T" denotes the transpose.

The only information available from the true system appears in the form of observed data. When data become available, they are used to form a correction to the forecast.

Assume that at a given time there are observations $\mathbf{w}_{k+1}^o$ available which are related to the true state vector $\mathbf{w}_{k+1}^t$ by

$$\mathbf{w}_{k+1}^o = \mathbf{H}_{k+1}\mathbf{w}_{k+1}^t + \mathbf{b}_{k+1}^o \tag{1}$$

where $\mathbf{b}_{k+1}^o$ is the observation error which is assumed to be a white sequence with zero mean and covariance given by $\left\langle \mathbf{b}_{k+1}^o \mathbf{b}_{k+1}^{oT} \right\rangle = \mathbf{R}_{k+1}$. $\mathbf{H}_k$ is the linear transformation which relates the state variables, in this case the Kelvin and Rossby wave amplitudes, to the observed quantities, at time t_k. In order to form the correction we must estimate the forecast error covariance

$$\mathbf{P}_{k+1}^f = \left\langle \left(\mathbf{w}_{k+1}^t - \mathbf{w}_{k+1}^f\right)\left(\mathbf{w}_{k+1}^t - \mathbf{w}_{k+1}^f\right)^T \right\rangle$$

If the error covariance of the analyzed field at time t_k is

$$\left\langle (\mathbf{w}_k^t - \mathbf{w}_k^a)(\mathbf{w}_k^t - \mathbf{w}_k^a)^T \right\rangle = \mathbf{P}_k^a$$

we may calculate

$$\mathbf{P}_{k+1}^f = \mathbf{L}\,\mathbf{P}_k^a\,\mathbf{L}^T + \mathbf{Q}_{k+1} \tag{2}$$

The updated state vector, the analysis, is taken to be a linear combination of the forecast and the observations. Write

$$\mathbf{w}_{k+1}^a = \mathbf{w}_{k+1}^f + \mathbf{K}_{k+1}(\mathbf{w}_{k+1}^o - \mathbf{H}_{k+1}\mathbf{w}_{k+1}^f) \tag{3}$$

where $\mathbf{K}_{k+1}$ is the Kalman gain matrix:

$$\mathbf{K}_{k+1} = \mathbf{P}_{k+1}^f \mathbf{H}_{k+1}^T \left(\mathbf{H}_{k+1}\mathbf{P}_{k+1}^f \mathbf{H}_{k+1}^T + \mathbf{R}_{k+1}\right)^{-1}$$

The error covariance of the updated field is given by

$$\mathbf{P}_{k+1}^a = (\mathbf{I} - \mathbf{K}_{k+1}\mathbf{H}_{k+1})\mathbf{P}_{k+1}^f$$

It is clear from (2) that if there is no dissipation in the system, $\mathbf{P}$ may grow indefinitely in the absence of assimilation. Steady values of $\mathbf{P}$ arise from a balance between dissipation and random forcing by system noise (see discussion by *Miller* [1986]). In the model used here, the energetics of the physical model lead to steady states (see, e.g., *Cane and Sarachik* [1977]; see also MC, section 5b); specifically, energy is lost at the western boundary.

3. CONSTRUCTION OF THE SIMULATED DATA SET

The simulated data set was constructed by adding a random field to the monthly FSU pseudostress analysis for the years 1978-1983. The random field had covariance structure given by the best-fit $\mathbf{Q}$. The actual random numbers were generated by the IMSL pseudo-random vector generator GGNSM. This basic simulation will be referred to as the "reference data set" to distinguish it from the other simulations performed in the course of this project.

In MC the system noise covariance matrix $\mathbf{Q}$ was calculated by assuming that the model errors had statistically homogeneous Gaussian structure. The error statistics had three parameters: the variance, the zonal correlation scale and the meridional correlation scale. These parameters were estimated by a parameter sweep in which a given set of parameters was used to calculate $\mathbf{Q}$, which was, in turn, used to iterate (2) until the value of $\mathbf{P}_k^f$ converged to its equilibrium value $\mathbf{P}_\infty$. This value of $\mathbf{P}_\infty$ was then used to evaluate the sea level height error covariance matrix for the six island stations chosen for the assimilation experiment. The matrix so obtained was then compared to the covariance of the actual difference between observed and predicted sea level height, and the parameter values which yielded the closest fit were chosen as the error model for actual assimilation experiments. The criterion for closest fit was the matching of the two leading EOF's. If the model error is ascribed to error in the wind field, then the parameters chosen correspond to just over 2 m/s rms error with a zonal correlation scale of 10 degrees and a meridional correlation scale of 2°. These values are consistent with generally accepted values of wind error statistics [*Chelton and O'Brien*, 1982; *Halpern and Harrison*, 1982; *Halpern*, 1988; *Reynolds et al.*, 1989; *Harrison et al.*, 1989].

Errors with the given statistics account for all of the discrepancy between the model analysis and real data when they are available. The view that errors in the wind analysis dominate the error budget is consistent with the results of *Harrison et al.* [1989], who used five different wind products as inputs to a detailed nonlinear model and found differences in the resulting dynamic height fields which were comparable to the error magnitudes estimated in MC. Even so, the skeptical reader who wishes to assign a greater proportion of the error to the simplicity of the model than to errors in the wind is invited to do so. Such a shift in interpretation of the error has little effect on the conclusions reached here. The interpretation of the estimated errors as errors in the wind field is discussed by MC.

The first and most important consideration in any simulation experiment is relevance, i.e., there must be reason to believe that the simulation resembles the real ocean. This can only be established statistically. In this case, a number of statistics must be compared. The statistics of the difference between the reference field and the raw output of the model driven by FSU winds must be compared to the difference between the raw model output and the real data, and both must be compared to the a priori estimate generated through the use of equation (2). These numbers will almost certainly not be identical, and special tools must be employed to determine the expected deviation of sample statistics from their

expected values, and to decide whether differences between calculated statistics are significant.

The first check to be performed on the range of expected statistics from the simulation experiment is the calculation of statistics for comparison to the computed value of $\mathbf{P}_\infty$. It was discovered that convergence of the calculated statistics to their predicted values given by the elements of $\mathbf{P}_\infty$ was very slow. Even after a 6-year simulation, in which a new random field was generated each month, the calculated variances differed more than initially expected from the diagonal elements of $\mathbf{P}_\infty$. This can be understood in several ways. Figure 1*a* shows the diagonal elements of $\mathbf{P}_\infty$ corresponding to the first baroclinic mode Kelvin wave amplitudes plotted along with the calculated variances of the state variables resulting from forcing the model with the perturbations alone. Distinct perturbations were simulated by starting the random number generator with different seeds. Results from three realizations are shown here. Variances were calculated for the final two years of a three year run, the first year having been allowed for spinup. Comparison of any one of the sample variance curves with its expected value shown by the bold line in Figure 1*a* might lead one to mistrust the calculation, but it can be seen from this figure that the realizations from the different seeds differ more from one another than any of the three differs from $\mathbf{P}_\infty$ and the mismatch between the diagonal elements of $\mathbf{P}_\infty$ and the calculated variances increases in the direction of the wave propagation, as one would expect from the convergence process. Figure 1*b* shows statistics similar to those from 1a, but taken from the last six years of a seven year run. The statistics from the longer runs are much closer to one another and to $\mathbf{P}_\infty$ than those from the shorter ones.

Alternatively, we may consider each state variable as being the result of a random process. The variance from each realization will cluster about some underlying population variance. The statistics of the sample variances can be estimated by the bootstrap technique (see, e.g., *Efron and Gong* [1983]). An example of such a calculation is shown in Figure 1*c*. In that figure, error variances and the bootstrap derived error bars are graphed on the same axes with the corresponding diagonal elements of $\mathbf{P}_\infty$. In that figure it can be seen that $\mathbf{P}_\infty$ is within the estimated standard error of the calculated variances for most state variables. One might, in fact, object that $\mathbf{P}_\infty$ is too good an estimate of the variances, since the error bars are only one standard deviation wide, and thus the corresponding value of $\mathbf{P}_\infty$ would be expected to lie outside the error bars nearly one-third of the time.

4. THE SIMULATED OBSERVATIONS

Simulated sea level heights from island tide gauge stations and at the locations of moorings in the TOGA-TAO array are used in this study. These moorings provide real-time telemetry of wind speed, sea surface temperature and vertical temperature profile $T(z)$. The first deployment of wind and $T(z)$ instruments was in 1986. Further deployments (TOGA-TAO 2; see *Hayes* [1989]) are proposed.

Obviously, sea level heights are not available at mooring sites. In this study, we treat dynamic height and sea level as being perfectly correlated. *Rebert et al.* [1985] investigated the relation between sea level, thermocline depth, heat content and dynamic height in the tropical Pacific. For stations near the equator, they found the slope of the regression line relating sea level to 400-m dynamic height to be close to 1 except at Santa Cruz, where changes in dynamic height are only 77% of those in sea level. They conclude that sea level changes near the equator seem to reflect density changes above 400 m. The TOGA-TAO Atlas moorings measure temperature profiles down to 500 m, and therefore should provide consistent measurements.

Dynamic height data derived from moorings are assumed to have the same error characteristics as tide gauge data, i.e., the errors are assumed to correspond to sea level errors with rms amplitude 3 cm. When the two baroclinic modes are considered separately, the errors in the two modes are assumed to be uncorrelated, and the measurements of each mode are assumed to contribute equally to the total error. The separate contributions to the modes are thus assumed to have error variances of 4.5 cm^2. This is almost certainly optimistic. *Hayes et al.* [1985] estimated the errors in the calculation of amplitudes of vertical modes based on measurements similar to those available from the moorings. In that study, they assumed that the noise was dominated by high vertical modes, and estimated errors in the lowest three modes based on assumptions about the vertical mode energy spectrum. They found that, without additional information such as deep measurements, error variances of more than 60% of the total signal variance could be expected for the second mode, which was the most poorly resolved. This would translate to an error variance closer to 20 cm^2 for the second mode.

In the first of two experiments with the simulated TOGA-TAO array, data from the moorings are considered to be identical to that obtained from tide gauges. In the second experiment, an attempt is made to take into account the information about the vertical density structure available from the Atlas moorings. The model used here has two baroclinic modes, each of which contributes separately to the sea level height. In that second experiment, the separate contributions of the two baroclinic modes to the sea level height are made available at the mooring sites.

Two sources of dynamic height data are simulated in this study: island tide gauge stations and Atlas moorings from the TOGA-TAO array [*Hayes*, 1989]. Simulated data at twelve of the seventeen currently deployed TOGA-TAO mooring sites are used for verification and data assimilation. Four selected sites from the planned expansion of the TOGA-TAO array are used for verification of the results of assimilating data from the 12 moorings selected from the present TOGA-TAO array. The locations of all of the sites used in this study are shown in Figure 2; the reader should compare this to Figure 1 of MC. Six island tide gauge stations are used for assimilation and four additional island sites are used for verification, as in MC. Clearly, the addition of even the preliminary TOGA-TAO data set can be expected to improve the coverage significantly.

5. OBSERVING SYSTEM SIMULATION EXPERIMENTS (OSSE)

5.1. *Overview*

Four numerical experiments were performed in the course of this work: "UNF," an unfiltered run, in which the model was driven by the FSU winds alone; "ISL," a run in which sea level height data were assimilated from the reference

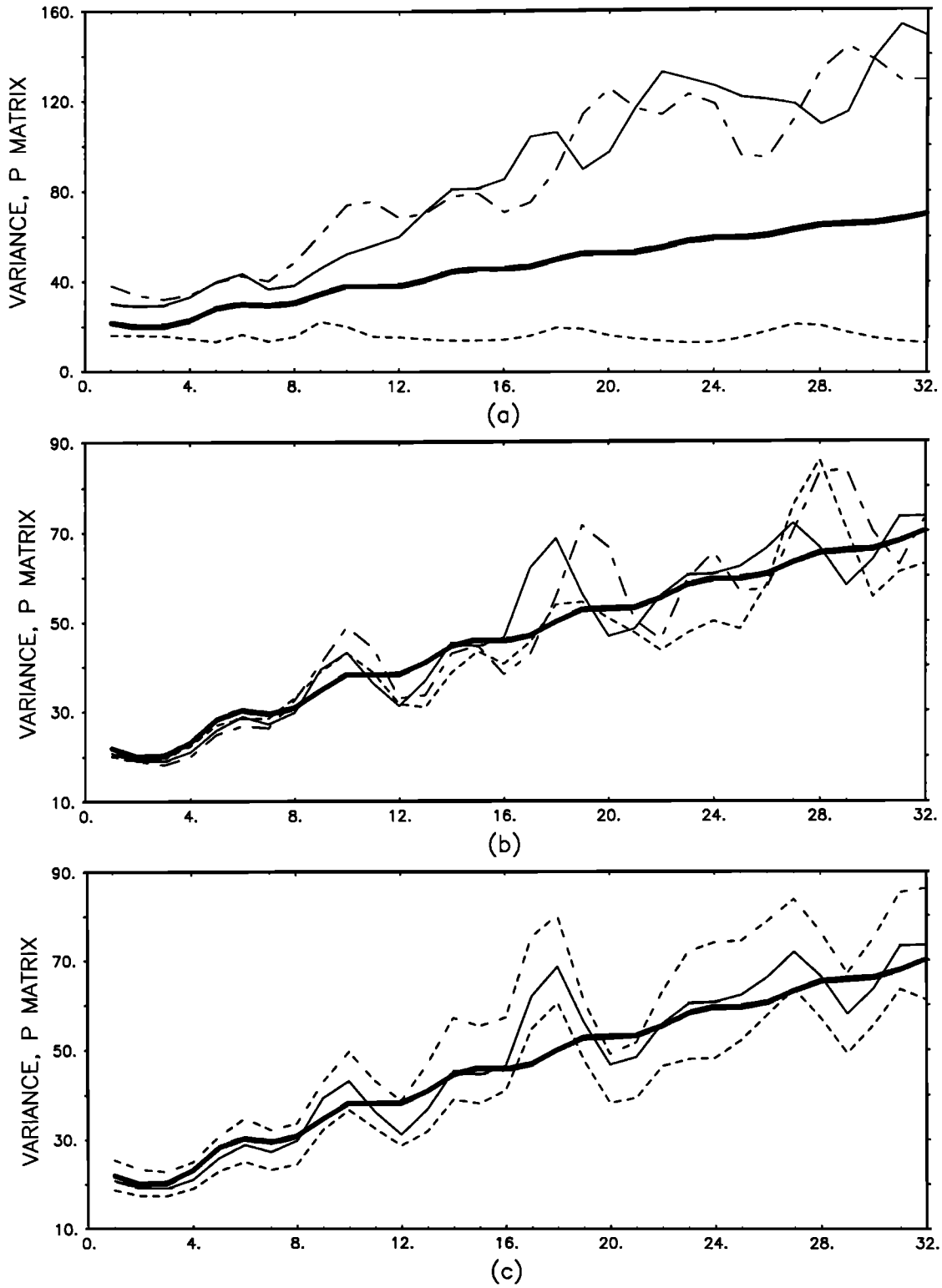

Fig. 1. Validation of the estimated error statistics. Convergence of statistical quantities to their estimated values. This figure shows the error variance of the first baroclinic mode Kelvin wave. Abscissa is the state variable index number; state variables are numbered from west to east. Heavy line: diagonal of **P** matrix, representing estimated error variance. (*a*): Variances of Kelvin wave amplitudes in simulations driven by random forcing. The thin solid line and the two dashed lines represent three different realizations. The three realizations were generated by a pseudo-random number generator using three different seeds. This panel represents two years of a three year simulation. (*b*): similar to Figure 1*a*, but for 6 years of a 7-year simulation. (*c*): heavy and thin solid lines as in Figure 1*b*. Dashed lines denote 68% confidence intervals about the thin solid line, calculated by the bootstrap method using 1000 bootstrap samples.

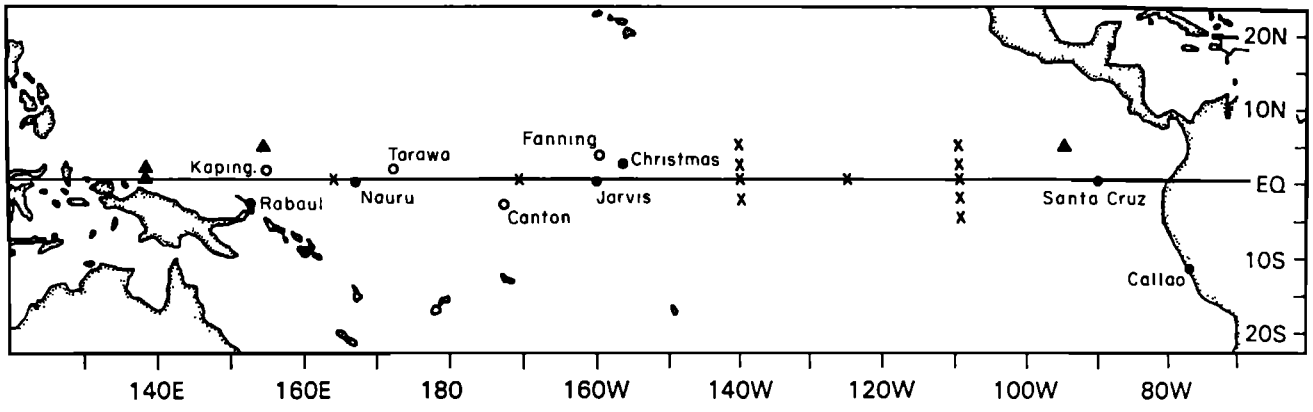

Fig. 2. The model domain, showing locations of tide gauge stations and TOGA-TAO Atlas moorings. Solid circles with labels are the primary assimilation sites. Open circles mark locations of tide gauge stations used for verification. Crosses denote currently occupied TOGA-TAO mooring sites used in assimilation experiments. These sites are designated TOGA-TAO 1 through TOGA-TAO 12 as follows: TOGA-TAO 1–5 are numbered from south to north at 110°W. TOGA-TAO 6 is on the equator at 125°W. TOGA-TAO 7–10 are numbered from south to north at 140°W. TOGA-TAO 11 and 12 are on the equator at 165°E and 170°W respectively. Solid triangles represent sites from the proposed expansion of the TOGA-TAO array. Simulated data from these sites are used for verification experiments.

data set at six island stations; "TOGA," in which sea level height data were assimilated at the six island tide gauge stations and the twelve selected TOGA-TAO mooring sites, and "BARO," in which separate contributions to the sea level heights from the two baroclinic modes were assimilated at the same TOGA-TAO locations used in "TOGA," along with sea level height data at the six island tide gauge stations. Due to greatly increased data coverage, TOGA and BARO are expected to outperform ISL and UNF. We shall see that, in fact, they do.

As noted in the introduction, the reference data set was the output from the model driven by the perturbed winds. OSSE were performed using the unperturbed FSU winds as input. Data for assimilation were taken from the reference data set. As an alternative, the output of the model driven by the unperturbed wind data set could have been used as reference data, and the perturbed winds used as input to the model for OSSE. The method used here was chosen because the perturbed wind stress data set will necessarily have greater variance than the unperturbed one, since the perturbations are uncorrelated with the FSU wind stress analysis. This is the more realistic case, since the FSU wind stress analysis contains considerable smoothing, and almost certainly underestimates the total wind stress variance.

5.2. *Assimilation of Simulated Island Station Data*

5.2.1. *Validation of MC: Is the structure of the dynamic height field really there?* The central experiment in MC can be duplicated by comparing the output of the unfiltered model (experiment "UNF") and the result of assimilating reference data at six island stations (experiment "ISL") with the reference data set. Here, as in MC, the Kalman filter was used to combine data from six island stations with the wind-driven model states. In MC, the observations were assumed to have 3 cm rms error. Random noise with 3 cm rms amplitude was therefore added to the reference heights at the island stations before assimilation.

The results of this first experiment are shown in Figures 3–6 and Tables 1–3. Figures 3–5 show the reference, unfiltered and filtered sea level height anomalies at the assimilation sites, the four island tide gauge stations used for verification and six of the TOGA-TAO mooring sites. The reference data plotted in Figures 3–5 are uncontaminated by observation noise. These figures are comparable to Figures 3 and 4 and Table 2 of MC. Figure 6 shows selected sea level height anomaly maps produced from all four experiments, along with the reference field. Tables 1 and 2 contain statistical summaries of the comparisons of model runs with simulated data at the ten island stations. Table 3 contains a statistical summary of the comparison of the model runs with simulated data at the twelve selected presently occupied TOGA-TAO sites. The statistics in Tables 1 and 2 are shown along with standard deviations calculated by the bootstrap method. Corresponding statistics from assimilation experiments in which real observations were used are shown for purposes of comparison.

The statistics in Table 1 were computed with noise imposed upon the simulated observations in order to facilitate comparison with similar error statistics derived from the earlier experiments using real data. In the case of comparison of filtered model output with noisy data, the correlation of the filtered state $\mathbf{w}_j^a$ with the observation noise $\mathbf{b}_j^o$ must be taken into account. This correlation results from the filtering process itself, as can be seen from (1) and (3). The formula for the error covariance at stations where updating actually occurs can be derived in straightforward fashion as follows:

$$\begin{aligned}\langle(\mathbf{w}_j^o - \mathbf{H}\mathbf{w}_j^a)(\mathbf{w}_j^o - \mathbf{H}\mathbf{w}_j^a)^T\rangle &= \langle\mathbf{H}(\mathbf{w}_j^t - \mathbf{w}_j^a) \\ &\quad + \mathbf{b}_j^o\left(\mathbf{H}(\mathbf{w}_j^t - \mathbf{w}_j^a) + \mathbf{b}_j^o\right)^T\rangle \\ &= \mathbf{H}\mathbf{P}_j^a\mathbf{H}^T - \mathbf{H}\mathbf{K}_j\mathbf{R} - \mathbf{R}\mathbf{K}_j^T\mathbf{H}^T + \mathbf{R} \\ &= \mathbf{R} - \mathbf{H}\mathbf{P}_j^a\mathbf{H}^T\end{aligned}$$

where the identity

$$\mathbf{K}_j = \mathbf{P}_j^a\mathbf{H}^T\mathbf{R}^{-1}$$

was used in the last step.

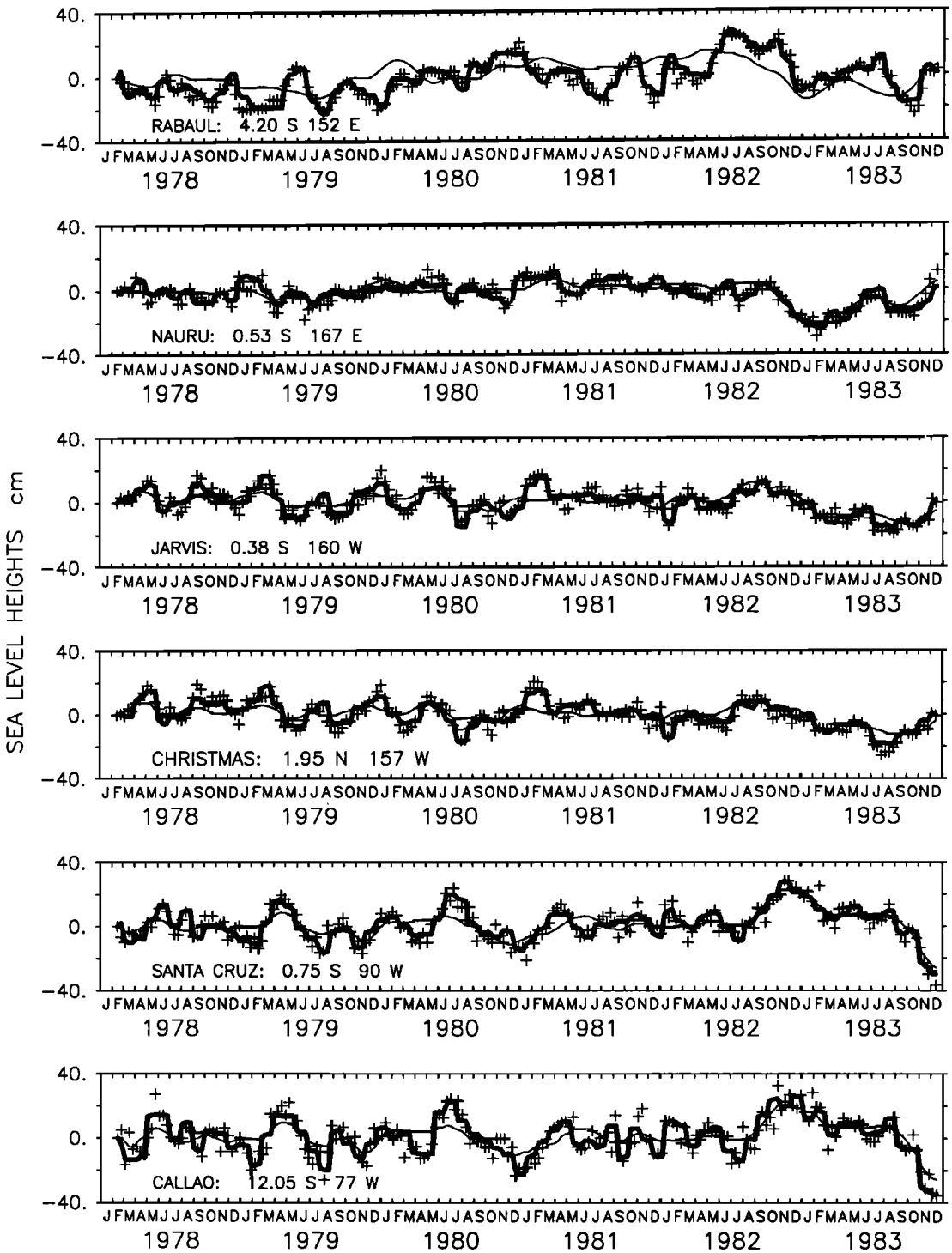

Fig. 3. Comparison of observation, raw model output and filtered output at island tide gauge stations participating in the assimilation. Heavy line: filtered output (experiment ISL); thin line: raw model output (experiment UNF); "+": reference data.

In the comparisons with real data in MC, the real observations had greater variance than sea level heights derived from the unfiltered simulation. In the simulation experiment, i.e., the reference sea level heights, which are the proxies for the real data, had greater variance than those derived from UNF. Maps of the total variance of the sea level signal are shown in Figure 7. While the same general pattern appears in all of them, the variance of the reference solution is nearly twice that of the unfiltered output over most of the basin. The only exception is in the southwest, where the variances are comparable in all of the simulations. As noted above, the greater variance of the reference solution was a consequence of the way the reference data set was constructed.

The statistical results from the comparisons of the reference island tide gauge data to unfiltered and filtered

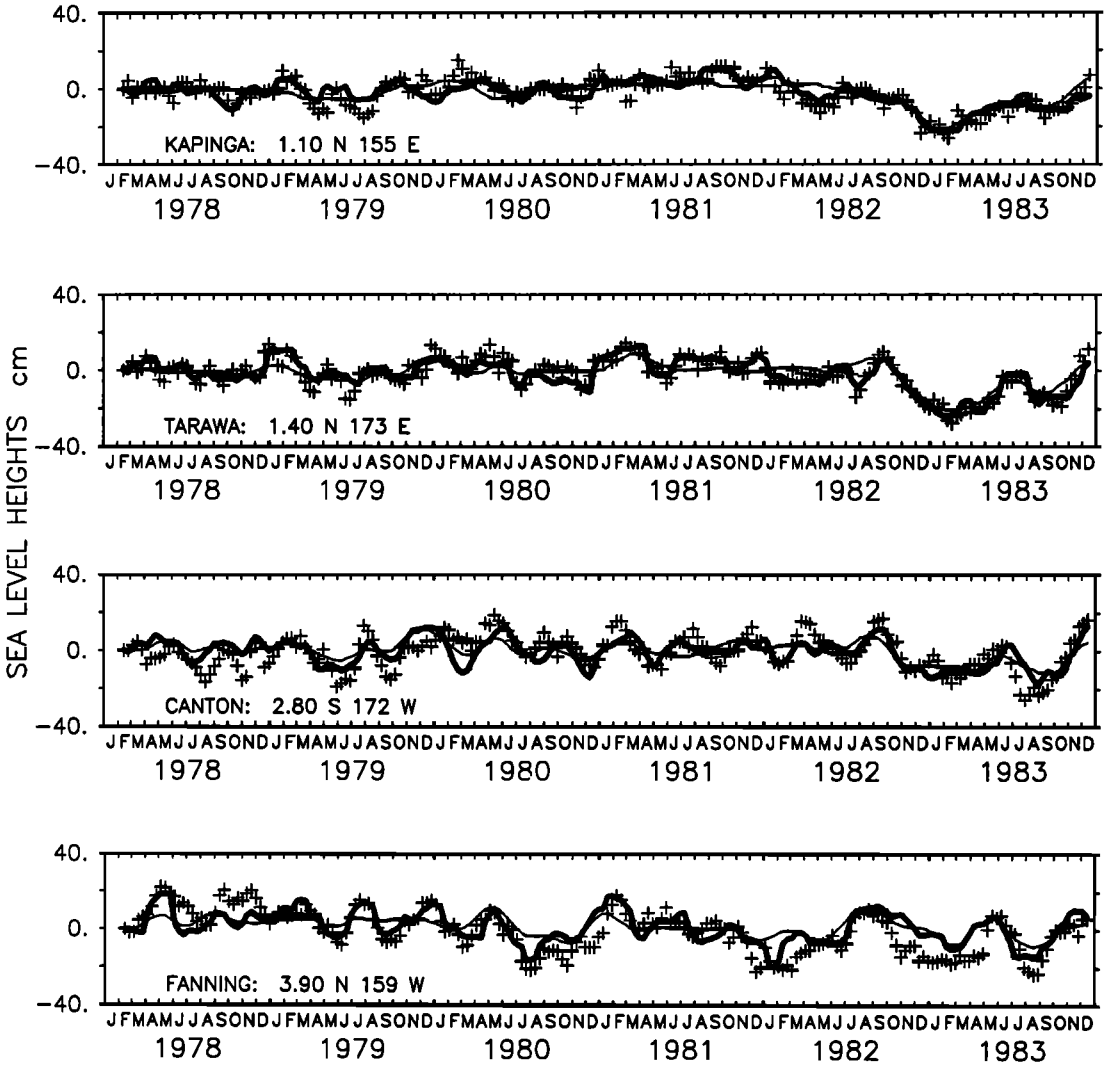

Fig. 4. Comparison of reference data, raw model output and filtered output at island tide gauge stations not participating in the assimilation. Heavy line: filtered output (experiment ISL); thin line: raw model output (experiment UNF); "+": reference data.

model output are summarized in Tables 1 and 2. In Table 1, the estimated error variances are shown, along with the actual tabulated error variances and the bootstrap estimates of the variance of the tabulated error variance about the population error variance. Statistics from the real data run (here denoted "OBS;" see also Table 2 from MC) are also included for comparison. Some small discrepancies will be noted from Table 2 of MC because of a slightly different method of calculating sample statistics. Examination of Table 1 shows that the σ intervals about the error variances in UNF relative to the reference data set and those relative to actual observed data overlap at six of the 10 island stations. The variances of the errors in the unfiltered run were actually greater in the comparison to the reference data than they were in comparison to actual observations in seven out of ten cases. These statistics reinforce the case originally presented in MC that the error bounds derived from the prior estimate of $\mathbf{Q}$ are reliable; they may even be conservative.

Sample correlation values are shown in Table 2, along with corresponding statistics from model runs with real data. In most cases, the correlations of the model output with the real observations were either within a standard deviation of the correlations with the simulated observations, or they were significantly higher. The only exceptions were in the unfiltered comparisons at Fanning, Kapingamarangi, and Callao.

The comparison between the reference sea level heights and runs UNF and ISL for the six islands at which assimilation took place is shown in Figure 3. As expected, the filtered sea levels are almost identical to the reference.

Figure 4 shows a similar comparison for the four island tide gauge stations where data were withheld from the filter. Since these data come from a simulation, they are not gappy as the real observations at these locations are, and not subject to the bias troubles that accompany gappy data. The filter performs well at Tarawa and Kapingamarangi, but provides no measurable improvement at Canton and Fanning. At Canton, the σ intervals about the filtered and unfiltered error variances overlap.

Comparisons between the reference data and the model output at a number of sites selected from the currently

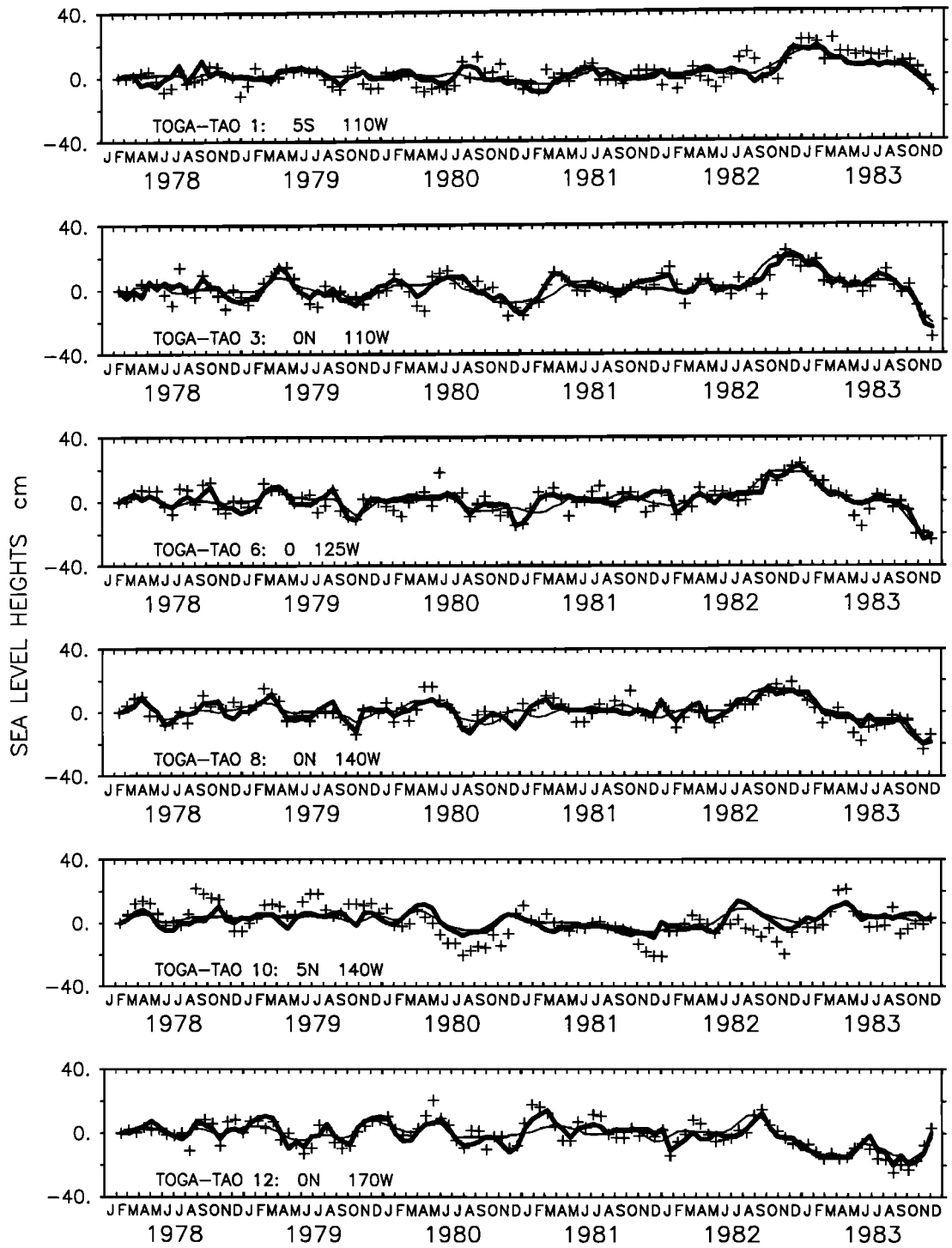

Fig. 5. Comparison of reference data, raw model output and filtered output at TOGA-TAO mooring sites. Heavy line: filtered output (experiment ISL); thin line: raw model output (experiment UNF); "+": reference data.

deployed TOGA-TAO array are shown in Figure 5 and Table 3. The filter has greatest effect at mooring number 12. This is an expected result, since this mooring is located near Tarawa, where the model also did well. Examination of the results from moorings 1, 5 and 10 shows that the filter has little effect at those stations farthest from the equator, as expected. Significant improvement can be noted at mooring number 3, indicating that the filter does some good in the data void between the Galapagos and 160°W. Further into that data void along the equator, at moorings 6 and 8, at 125°W and 140°W respectively, the filter has rather less effect. In both of these records, the filtered analysis misses a large spike in the spring of 1980, and misses a large negative response during the 1982-83 ENSO event.

Figure 6 shows selected contour maps from all four experiments of the sea level height field for the sixth year of the simulation. The reference field is also shown for

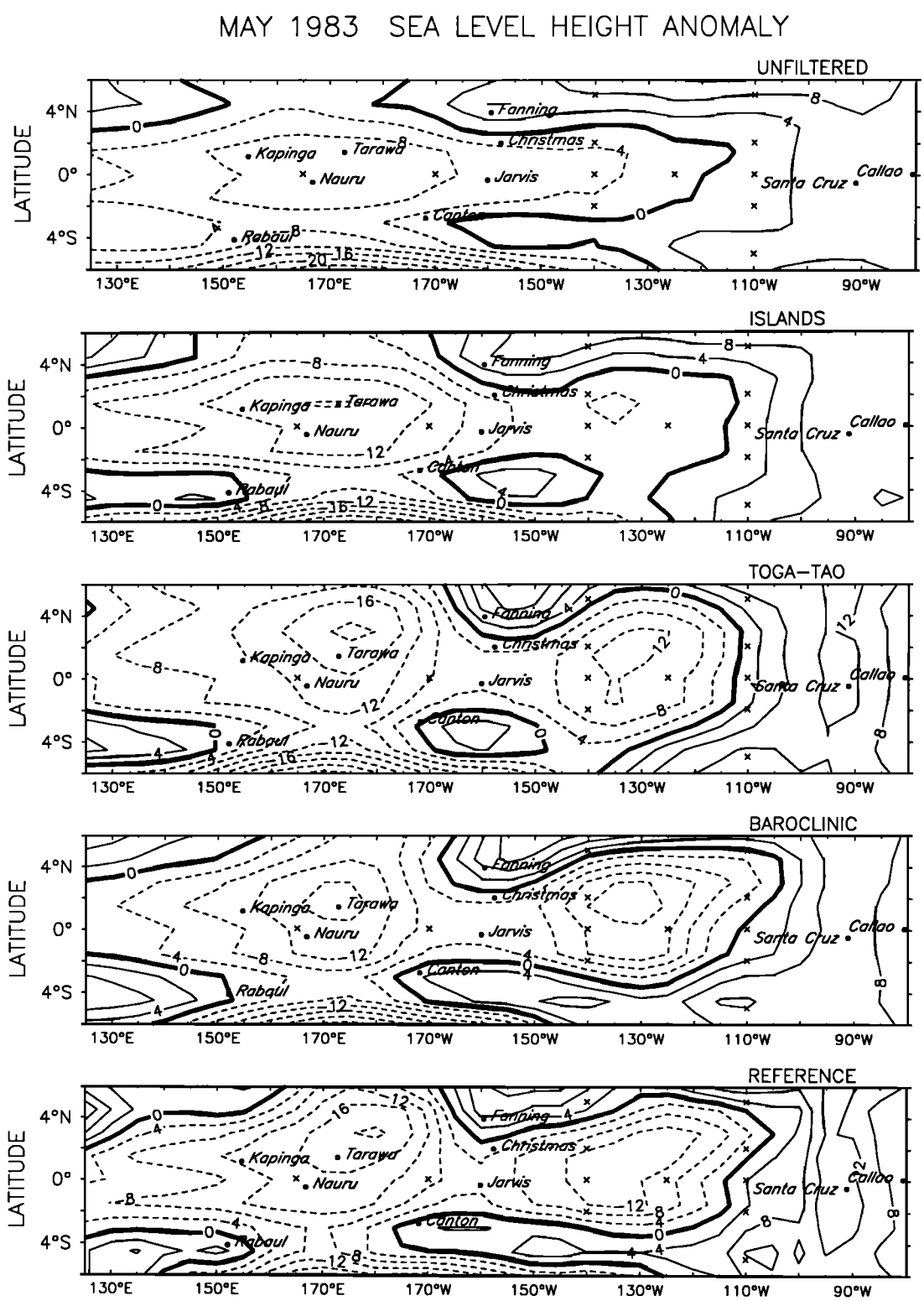

Fig. 6. Contour maps of sea level anomaly for the months of May and July of 1983 from the four model simulations, along with the reference field. In the "ISL" experiment, data were assimilated at Rabaul, Nauru, Jarvis, Christmas, Santa Cruz and Callao. In the "TOGA-TAO" experiment, data were assimilated at 12 of the TOGA-TAO mooring sites, marked by "x," along with the six island stations from the previous experiment. In the "BAROCLINIC" experiment, the contributions to the dynamic height from the two baroclinic modes were assimilated as separate items. Contour levels are in centimeters.

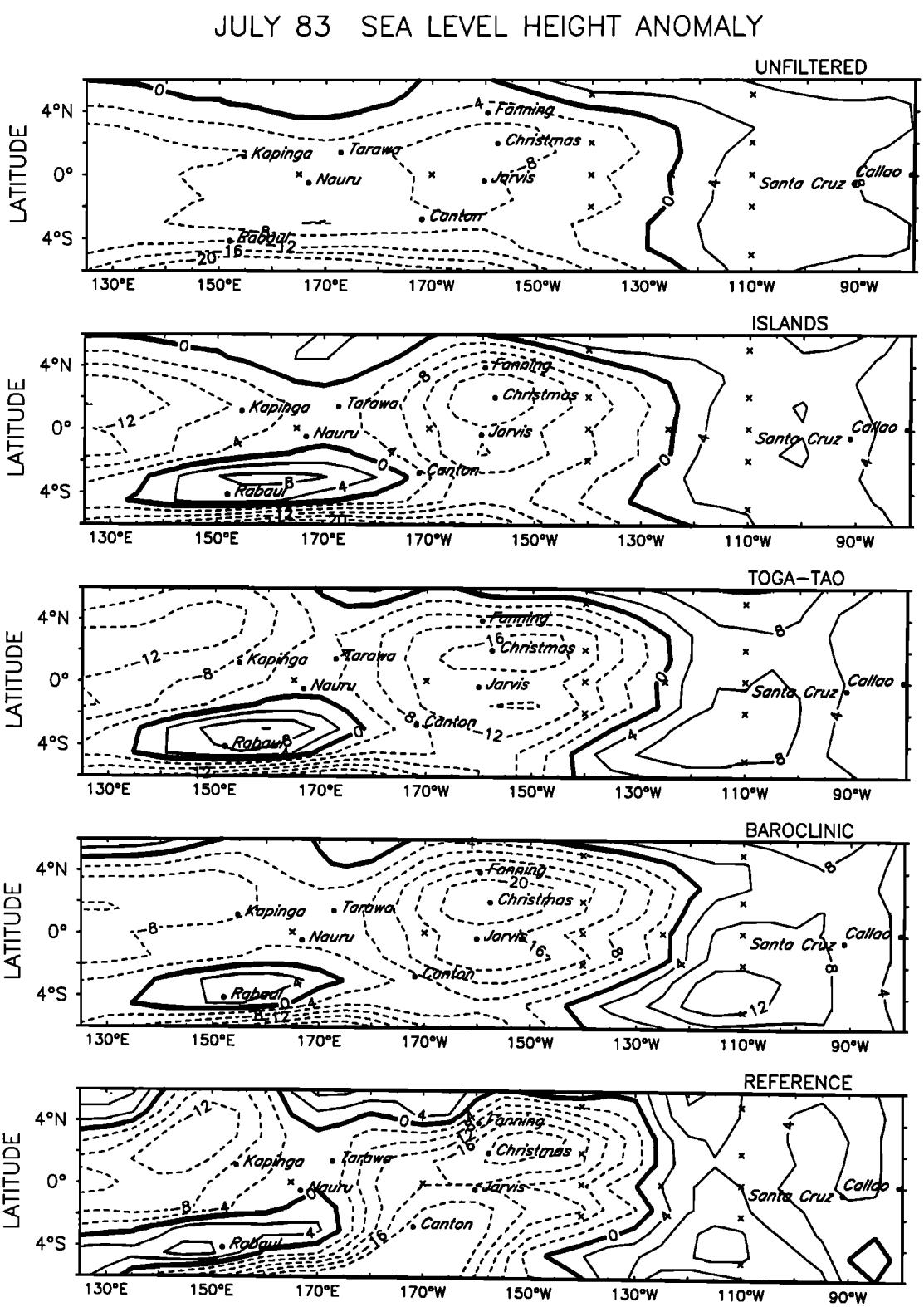

Fig. 6. (continued)

comparison. Application of the filter at six island stations (experiment "ISL") has comparatively little effect on the height field for May. As noted from the comparisons to the reference mooring data, it fails to pick up the low along the equator near 125°W. The filter does make some difference along the western boundary, where it corrects the analysis in the positive direction in the north and south. The effect of the filter in July is more pronounced. Though it again fails to reproduce structure in the data void near 120°W, it does intensify the negative anomaly just north

TABLE 1. Variances of Calculated and Observed Sea Level Heights and Sea Level Height Errors

			UNFILTERED (No Assimilation)				ISLANDS (Assimilation at Six Islands)			
Station	OBS[a]	Reference[b]	Total[c]	UNF-REF[d]	UNF-OBS[e]	EST[f]	Total[g]	ISL-REF[h]	ISL-OBS[i]	EST[j]
Rabaul	59(9)	140(22)	68(8)	131(19)	45(8)	98	121(20)	1.6(0.2)	0.53(0.2)	3
Nauru	116(22)	71(13)	40(10)	32(4)	54(9)	39	58(12)	2.2(0.4)	2.8 (0.5)	3
Jarvis	68(14)	77(12)	36(6)	42(8)	23(4)	40	63(9)	3.4(0.5)	2.1 (0.3)	5
Christmas	99(22)	71(13)	27(5)	39(8)	50(12)	46	61(10)	2.3(0.4)	2.2 (0.5)	4
Santa Cruz	117(26)	120(24)	67(17)	47(8)	59(10)	51	112(23)	2.2(0.4)	3.9 (0.8)	3
Callao	73(19)	177(35)	63(16)	70(10)	54(10)	78	153(31)	2.0(0.3)	0.77(0.1)	2
Kapinga	35(6)	68(11)	39(9)	30(5)	26(4)	43	51(11)	23 (4)	29 (6)	24
Tarawa	77(15)	85(17)	43(10)	39(10)	24(5)	44	68(13)	20 (4)	13 (3)	19
Canton	60(12)	95(14)	26(4)	64(8)	49(14)	60	47(7)	50 (6)	32 (7)	39
Fanning	63(15)	101(14)	22(4)	62(9)	58(12)	75	65(10)	45 (7)	16 (3)	46

Values are in square centimeters; figures in parentheses are bootstrap standard deviations based on 1000 bootstrap samples.

[a]Total variance, i.e., mean square amplitude of observed sea level height anomaly.

[b]Total variance for the reference data set.

[c]Total variance for experiment UNF.

[d]Variance of the series of differences between the output of experiment UNF and the reference data set.

[e]Variance of the series of differences between the output of experiment UNF and observed data.

[f]The a priori estimate of the variance of UNF-REF and UNF-OBS generated by the Kalman filter.

[g]Total variance for experiment ISL.

[h]Variance of the series of differences between the output of experiment ISL and the reference data set.

[i]Variance of the series of differences between the output of experiment ISL and observed data but for a model run with assimilation of actual observations at six island stations.

[j]The a priori estimate of the variance of ISL-REF and ISL-OBS generated by the Kalman filter.

TABLE 2. Correlations of Calculated Sea Level Heights With Reference Data and With Observations

	UNFILTERED (No Assimilation)		ISLANDS (Assimilation at Six Islands)	
Station	UNF-REF[a]	UNF-OBS[b]	ISL-REF[c]	ISL-OBS[d]
Rabaul	0.39(.06)	0.64(0.08)	0.99(0)	1.0 (0)
Nauru	0.72(.04)	0.75(0.08)	0.98(0)	0.99(0)
Jarvis	0.67(.03)	0.81(0.05)	0.98(0)	0.99(0)
Christmas	0.68(.03)	0.74(0.06)	0.98(0)	1.0 (0)
Santa Cruz	0.76(.04)	0.71(0.07)	0.99(0)	0.99(0)
Callao	0.78(.03)	0.61(0.08)	1.0 (0)	1.0 (0)
Kapinga	0.72(.04)	0.54(0.12)	0.81(0.03)	0.81(0.06)
Tarawa	0.73(.05)	0.83(0.05)	0.87(0.02)	0.93(0.02)
Canton	0.55(.05)	0.47(0.13)	0.63(0.04)	0.74(0.06)
Fanning	0.63(.04)	0.36(0.12)	0.73(0.03)	0.90(0.03)

Values in parentheses are bootstrap standard deviations based on 1000 bootstrap samples.

[a]Correlation of heights from experiment UNF with reference heights.

[b]Correlation of heights from experiment UNF with observed data.

[c]Correlation of heights from experiment ISL with reference heights.

[d]Correlation of observed heights with experiment ISL with assimilation of actual observations at six island stations.

of the equator near 160°W, and correctly places a positive anomaly in the southwest which does not appear in the unfiltered map.

Assimilating data at the six island stations results in some improvement, but misses some important features and underestimates others. The structure observed in the assimilation experiment in MC was probably really there. The actual structure was probably richer still.

5.2.2. *Effect of assimilating data at the TOGA-TAO mooring sites.* Since data are now available in real time from the Atlas moorings at the TOGA-TAO locations shown, it is reasonable to perform an OSSE using data at those sites. In the second experiment in this series (the experiment "TOGA"), sea level height data (as proxy for the 500-m dynamic height data actually available from the moorings) are assumed to be available at the 12 presently

TABLE 3. Summary Statistics From Selected TOGA-TAO Moorings

Site	Latitude, deg	Longitude, deg	Total Variances			Error Variances				Correlations	
			REF[a]	UNF[b]	ISL[c]	UNF-REF[d]	EST[e]	ISL-REF[f]	EST[g]	UNF-REF[h]	ISL-REF[i]
1	5S	110W	67	27	33	35	46	30	36	0.70	0.74
2	2S	110W	71	49	57	27	37	17	24	0.79	0.88
3	0	110W	81	55	64	33	36	17	23	0.77	0.89
4	2N	110W	66	47	85	29	37	18	24	0.76	0.72
5	5N	110W	63	37	82	34	46	33	36	0.68	0.35
6	0	125W	82	54	54	32	35	24	23	0.78	0.84
7	2S	140W	59	27	25	34	40	29	26	0.65	0.76
8	0	140W	67	40	42	30	34	20	19	0.74	0.84
9	2N	140W	59	28	31	35	40	26	26	0.64	0.75
10	5N	140W	90	20	30	65	64	65	56	0.53	0.51
11	0	165E	76	44	60	24	30	12	6	0.83	0.95
12	0	170W	89	42	65	34	31	20	14	0.79	0.91

Variances are in square centimeters. EST columns represent a priori estimated error variances.
[a]Total variance for the reference data set.
[b]Total variance for experiment UNF.
[c]Total variance for experiment ISL.
[d]Variance of the series of differences between the output of experiment UNF and the reference data set.
[e]The a priori estimate of the variance of UNF-REF generated by the Kalman filter.
[f]Variance of the series of differences between the output of experiment ISL and the reference data set.
[g]The a priori estimate of the variance of ISL-REF generated by the Kalman filter.
[h]Correlation of heights from experiment UNF with reference heights.
[i]Correlation of heights from experiment ISL with reference heights.

occupied TOGA-TAO mooring sites shown in Figure 2, in addition to the six island tide gauge stations used in ISL. Simulated errors in the form of white noise with 3 cm rms amplitude are added to the reference data before they are assimilated. The other four island stations are again held back for verification. Maps of sea level anomaly for May and July 1983 calculated from this run are shown in Figure 6.

In the May map, the most obvious effect of including data at the TOGA-TAO sites is observed in the eastern half of the basin. In this run, the strong negative anomaly centered just north of the equator near 130°W, which is very nearly absent from the ISL analysis, appears. In the July map, the negative anomaly near 150°W is well represented in ISL, and the addition of the TOGA-TAO data adds little. In the northwest, however, the negative anomaly is correctly extended to the northern boundary in TOGA, while in ISL, there is even a small positive anomaly near the northern boundary at 170°E.

Little additional detail is provided by separate assimilation of the two baroclinic modes (experiment "BARO"). In BARO, the eastward extent of the negative anomaly near 130°W is slightly better represented than it is in TOGA in both May and July. BARO also reproduces the positive anomaly in the northwest in the May map. This feature is absent from TOGA, despite its presence in UNF and ISL. The fact of TOGA being a bit worse than UNF and ISL at this particular time and place is due to the particular realization of the simulated observation error. The reader should bear in mind the fact that real instrument errors will occasionally have this effect.

Maps of expected rms errors in sea level height are shown in Figure 8. As in MC, the improvement in ISL over UNF is noticeable, but not dramatic. The effect of assimilation of data from the TOGA-TAO moorings (experiments "TOGA" and "BARO") is quite significant. Expected rms errors are near 3 cm over much of the basin near the equator. This is the same as the assumed rms observational error, and is thus about the same level as would be obtainable from a dense network of tide gauges. The interpretation of estimated errors less than the 3 cm data error level is questionable, since estimates in that range depend on the details of the system noise model. Expected rms errors from experiment BARO differ only in fine detail from those from TOGA. It can be seen from this figure that there was little room for improvement.

When the TOGA-TAO data are added to the system, the filter weights the island stations correspondingly less in the analysis, and decreases the range of the influence of the island stations on the analysis. In TOGA and BARO, data are available between the Galapagos and 160°W so it is not necessary to rely on data from Jarvis, Christmas, or Santa Cruz to correct the forecasts in the data void. From (3) we see that the correction to the forecast sea level height at a given point in the model domain is a weighted sum of the differences between the observed and forecast sea level heights at the islands where the tide gauges are located. Given an arbitrary fixed point in the domain, the influence of data at a given island station upon the analysis at that point is measured by the weight in the above-mentioned weighted sum. These weights, referred to as "influence functions" by *Ghil et al.* [1981], are shown as contour maps in Figure 9 for selected island stations. Larger weights represent greater influence. Negative weights indicate that

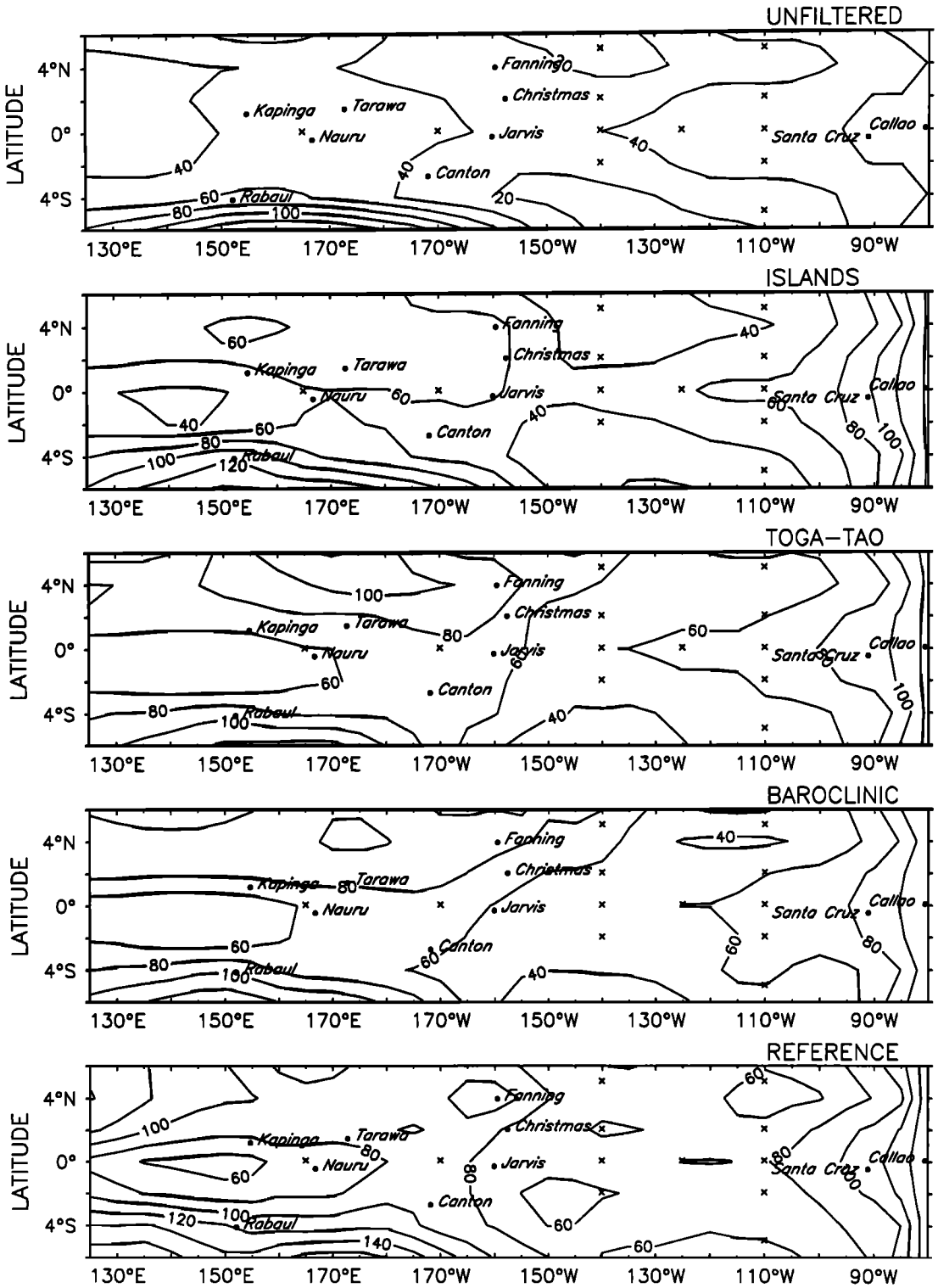

Fig. 7. Contour maps of total sea level variance about zero, for the last four years of a 5-year simulation. Contour levels are in square centimeters.

the sign of the correction is opposite to that of the forecast error at the island under consideration. Similar maps appear in Figure 8 of MC.

The influence of Christmas Island in ISL (Figure 9*a*) takes a maximum value greater than 0.45, and extends east of the TOGA-TAO mooring line at 140°W. In TOGA, however, (Figure 9b), the maximum influence of Christmas island is just over 0.3, and the range of influence is confined essentially to the west of 140°W. The slight negative influence just south of the equator near 170°W remains in both ISL and TOGA.

The influence of Santa Cruz (Figures 9*c* and 9*d*) appears

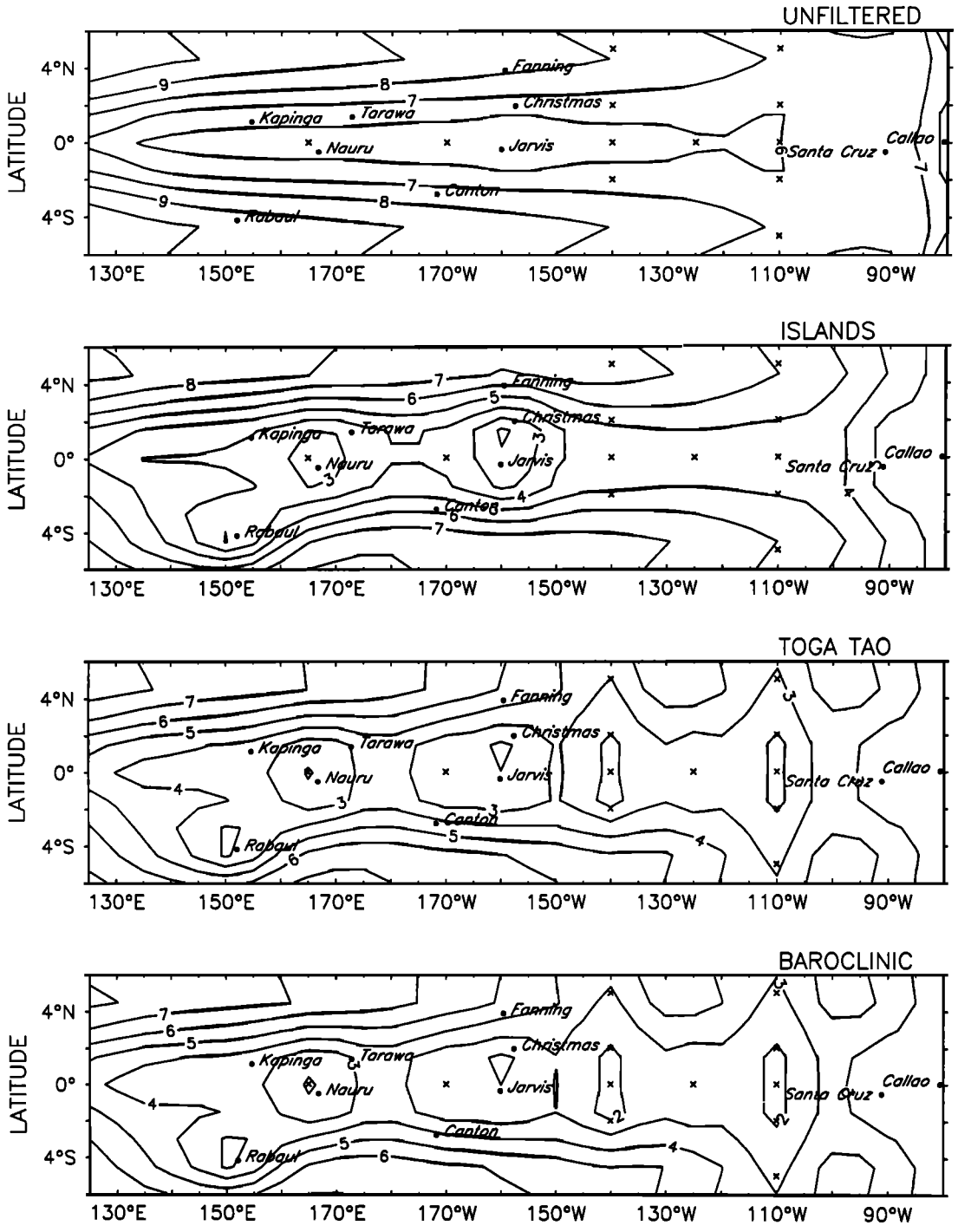

Fig. 8. Contour maps of expected rms error in sea level height anomaly. Contour levels are in centimeters.

to be responsible for much of the structure in the analysis in ISL in the data void between 90° and 160°W. In TOGA, the influence of Santa Cruz is mostly confined to the east of the TOGA-TAO mooring line at 110°W.

A statistical summary of the results of experiments ISL, TOGA and BARO at the four island stations where data were not assimilated and four of the proposed TOGA-TAO mooring sites (shown as filled triangles in Figure 2, and denoted TG2–1 through TG2–4) is shown in Table 4. The statistics in Table 4 were calculated using reference values uncontaminated by noise. The estimates based on the calculated covariance matrix have been adjusted accordingly. Of the stations recorded here, the greatest improvement in TOGA and BARO over ISL occurs at Canton and Fanning. There is no significant improvement at the four proposed TOGA-TAO–2 sites TG2–1 through TG2–4. At all four of those sites, error bars drawn one standard deviation wide about the measured error variance from ISL encompass the measured and estimated error variances form TOGA and BARO. This indicates

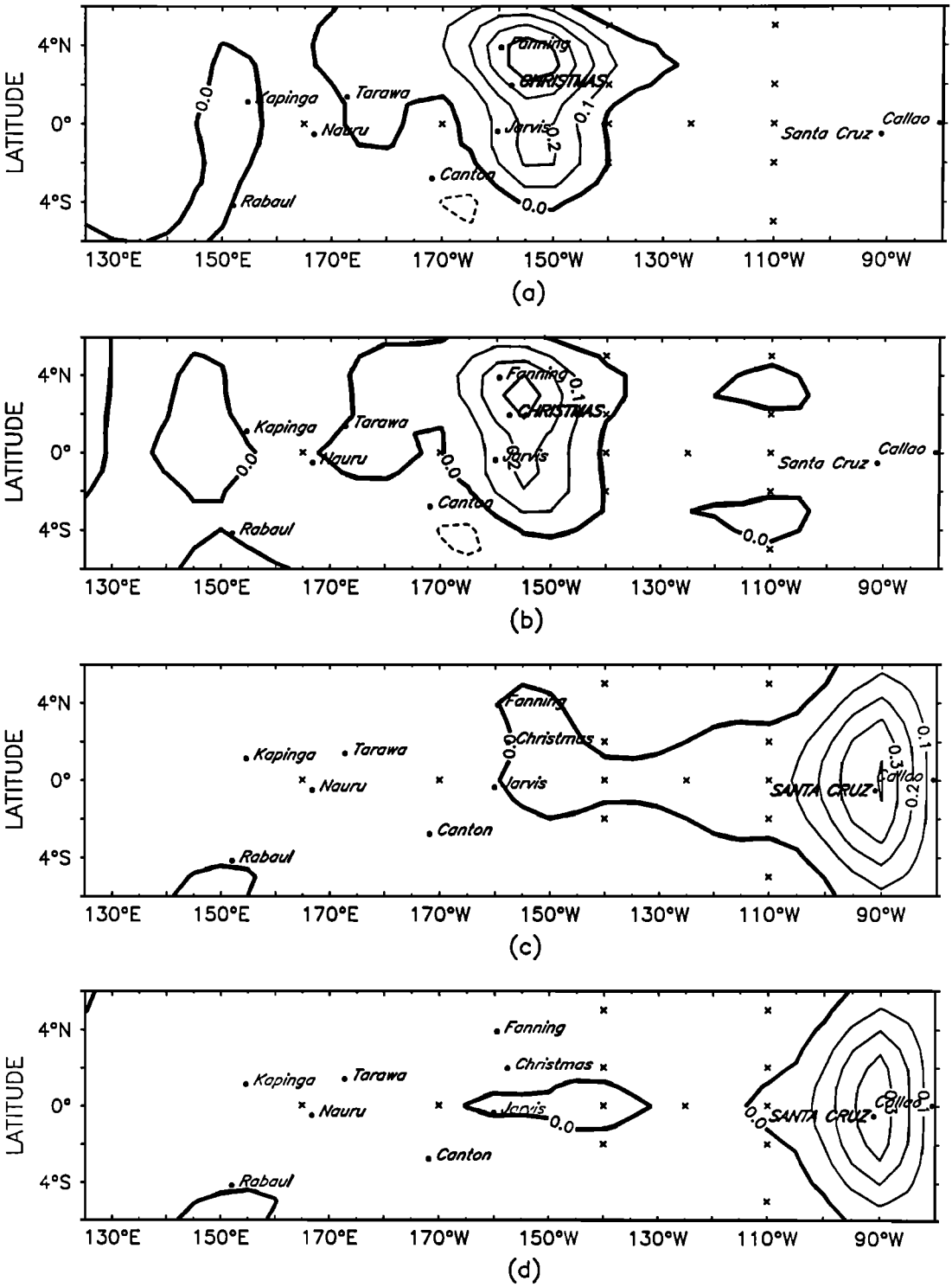

Fig. 9. Contour maps of influence of data at tide gauge stations, showing the general decrease in influence at each station from ISL, the experiment in which data from six island stations were used for assimilation, and TOGA, in which data from 12 TOGA-TAO moorings were added. The selected tide gauge location is noted on the map in boldface. (*a*) Influence of Christmas Island in ISL. (*b*) Similar to Figure 9*a*, but for TOGA. (*c*) Influence of Santa Cruz in ISL. (*d*) Similar to Figure 9*c*, but for TOGA.

that inclusion of measurements at the TOGA-TAO–2 sites should result in significant error reduction.

The error bars also overlap at Kapingamarangi and Tarawa. The difference from ISL to TOGA and BARO may be statistically significant at Tarawa because the estimated error variance from TOGA and BARO falls below the error bar about the error variance from ISL. The difference, however, is certainly of no practical importance. The numbers in Table 4 are consistent with Figure 8. From these results, it is clear that the greatest improvement is in

TABLE 4. Statistics From Assimilation of TOGA-TAO Data

Station	Latitude and Longitude, deg	Variance[a]	ISL-REF[b]	EST[c]	TOGA-REF[d]	EST[e]	BARO-REF[f]	EST[g]
Kapinga	1.1N 155E	68(11)	14(3)	15	12(2)	12	11(2)	11
Tarawa	1.4N 173E	85(17)	12(2)	10	9(2)	8	9(2)	8
Canton	2.8S 172W	95(14)	41(8)	30	19(4)	16	21(4)	15
Fanning	3.9N 159W	101(14)	32(5)	37	23(4)	19	20(3)	18
TG2-1	2 N 141E	86(13)	23(5)	24	19(4)	20	20(3)	19
TG2-2	0 141E	50(7)	15(3)	15	13(3)	13	13(2)	12
TG2-3	5 N 155E	85(14)	63(12)	74	70(12)	56	54(9)	54
TG2-4	5 N 95 W	65(12)	22(4)	22	21(4)	20	17(3)	19

Variances are in square centimeters. Figures in parentheses are bootstrap standard deviations based on 200 bootstrap samples. TG2 represents mooring sites in the proposed expansion of TOGA-TAO.
[a]Total variance of reference sea level height.
[b]Variance of differences between calculated and reference sea level heights for experiment ISL.
[c]A priori estimate of the variance of differences between calculated and reference sea level heights for experiment ISL.
[d]Variance of differences between calculated and reference sea level height for experiment TOGA.
[e]A priori estimate of the variance of differences between calculated and reference sea level heights for experiment TOGA.
[f]Variance of differences between calculated and reference sea level heights for experiment BARO.
[g]A priori estimate of the variance of differences between calculated and reference sea level height for experiment BARO.

the east-central part of the basin, where the TOGA-TAO 1 moorings have filled the data void which existed in ISL.

5.3. *Estimation of 20° Isotherm Depth Anomaly*

Thus far, only sea level height data have been considered. Since the model is formulated in terms of baroclinic modes, the depth of the thermocline, here taken to be the 20° isotherm, is represented as a linear combination of the amplitudes of the vertical modes, similar to the representation of the sea level height, but with different coefficients. Because the model responds qualitatively as a reduced gravity model, the sign of the 20° isotherm anomaly will be opposite that of the sea level height.

The computations used to generate the 20° isotherm anomaly maps are the identical ones used to generate the sea level height maps of the previous section. We expect, a priori, that the assimilation of the separate contributions of the vertical modes in experiment "BARO," will result in more accurate thermocline anomaly maps than the assimilation of sea level height data at those locations. Sea level height and the thermocline depth are different linear combinations of the same quantities; specifying the two quantities separately determines all linear combinations of those quantities, while specifying one particular linear combination does not.

Maps of the 20° isotherm depth anomaly for May and July of 1983 are shown in Figure 10. As in the case of the sea level height anomaly maps, the anomalies are, for the most part, too weak. One exception to this general rule is in the southwest corner of the May map. In that map in the southwest, the unfiltered response is in fact too strong, and assimilation of data at Rabaul weakens the anomalies considerably, correctly producing a region of near-zero anomaly that is absent in the unfiltered map. Assimilation of TOGA-TAO data improves the maps considerably in the eastern part of the basin, as expected, producing the positive anomaly near 130°W which does not appear in 'the maps with data assimilated from island stations alone.

In the July maps, the unfiltered map shows very little structure. Filtering at six stations results in considerable improvement in most of the region, but strengthens the erroneous negative anomaly in the northwest and overpredicts the anomaly in the southwest. This is corrected by assimilation of the TOGA-TAO data, but even with the assimilation of the mooring data, the negative anomaly in the southwest is overpredicted. As expected, the assimilation of the mooring data improves the maps significantly between 90° and 160°W.

The expected rms errors for the four runs are shown in Figure 11. In the unfiltered run, the expected errors along the equator are about 16 m over most of the basin, increasing sharply away from the equator and toward the western boundary. Filtering at six stations improves the analysis noticeably, reducing the overall errors to about 12 m, decreasing to 8 m near the assimilation stations. With the addition of the TOGA-TAO moorings, the expected rms errors remain around 8 m across the most of the basin along the equator, decreasing to 6 m near the data gathering sites. Assimilation of the separate baroclinic modes results in very little improvement. The more accurate regions near the data gathering sites broaden a bit, but the effect is probably not discernible in practice.

A summary of error variances at selected stations not participating in the assimilation is shown in Table 5. There may be significant improvement in TOGA and BARO over ISL at TG2–3, where the error estimate is high, and the calculated error variance for this realization may be far from the ensemble mean. There may also be significant improvement in BARO, but not TOGA, over ISL at TG2–2, but this is probably of no practical importance. The greatest improvement is at Canton and Fanning, where TOGA and BARO represent a large improvement over ISL, but differ little from one another.

6. CONCLUSIONS

A simulated data set was produced by driving a dynamical model with a wind field obtained by perturbing the FSU wind data set. The parameters used in generating

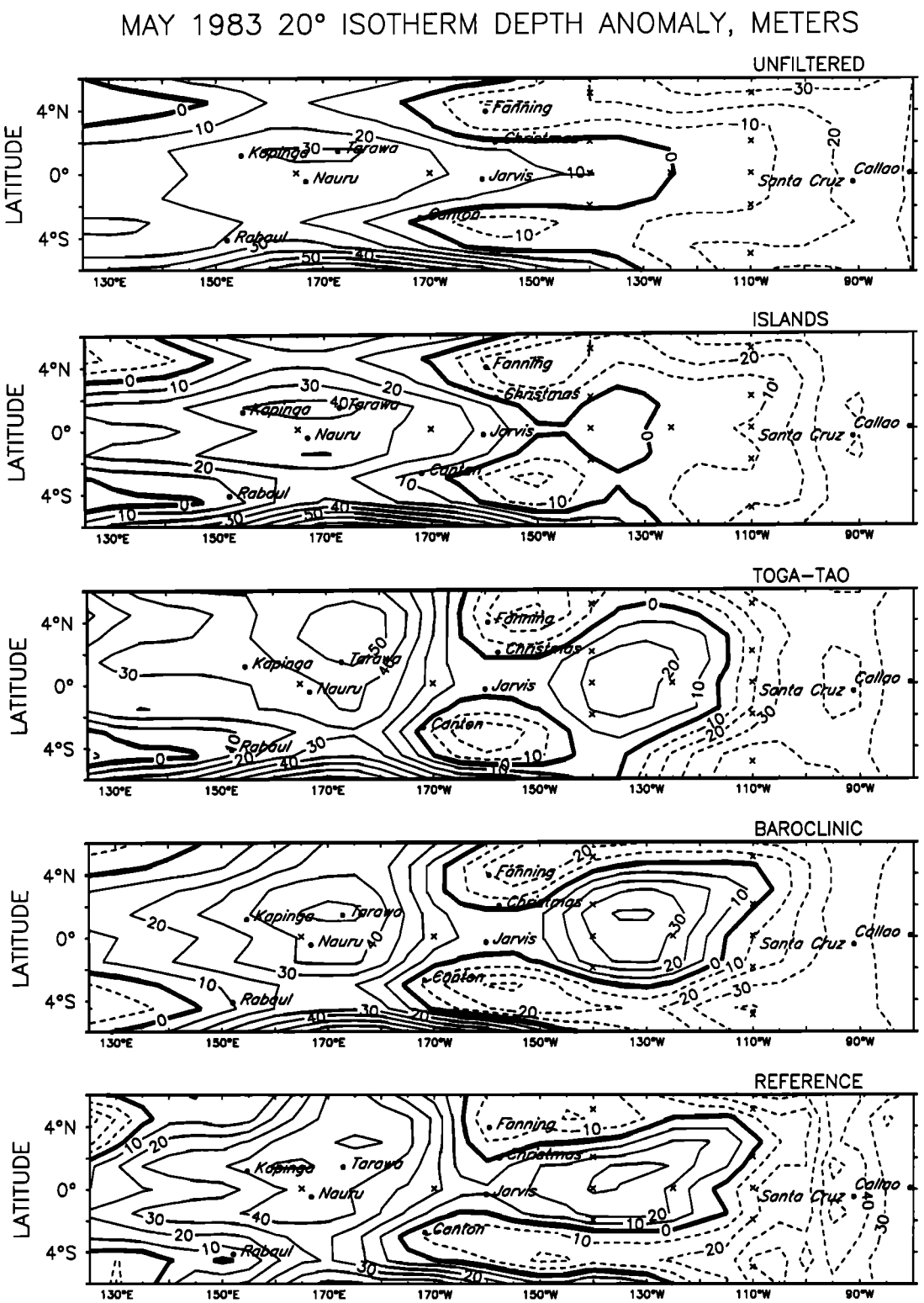

Fig. 10. Contour maps of 20° isotherm depth anomaly for the months of May and July of 1983 from the model simulation. Contour levels are in meters.

the random perturbations were determined by an earlier analysis of errors in the wind data set (see MC). Simulated observations at selected island stations and TOGA-TAO mooring sites were used to perform OSSE.

The Kalman filter was used to assimilate data in these experiments. Other assimilation methods would have produced similar results. It is well known that the Kalman filter is equivalent to a particular inverse calculation; see, e.g., *Bennett and Budgell* [1989].

An optimal interpolation method similar to those used in numerical weather prediction (see, e.g., *Schlatter et al.* [1976]) might well have proved satisfactory for this

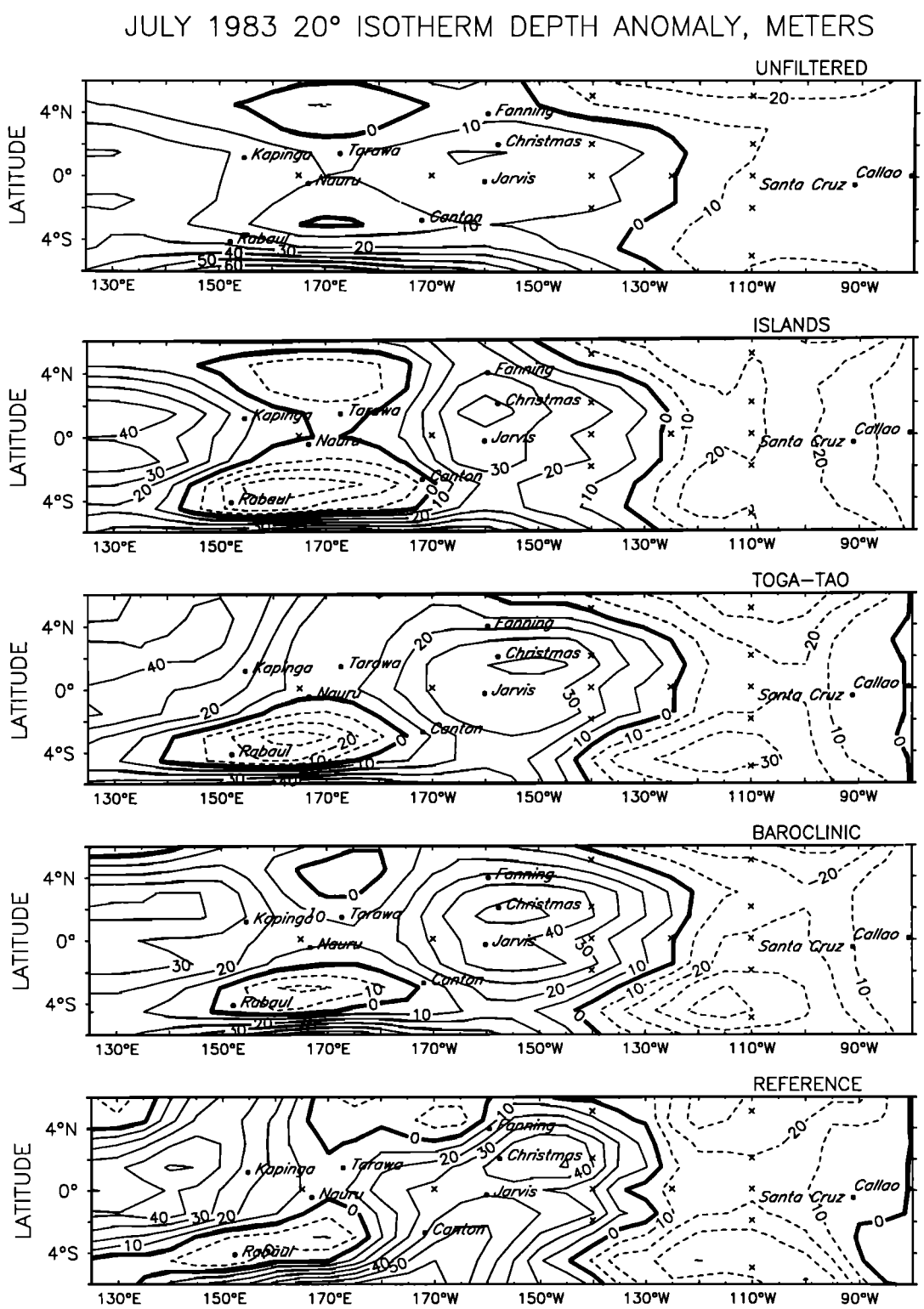

Fig. 10. (continued)

study, but it would have been necessary to expend a fair amount of effort on the design of such a scheme. Optimal interpolation methods are similar to the Kalman filter in that a correction to the forecast field is calculated according to (3), but an assumed form of the error covariance matrix **P** is used to calculate the gain matrix. In cases such as this one, in which **P** eventually converges, the function of the Kalman filter is identical to optimal interpolation once that convergence is achieved, though one would be unlikely to arrive at the converged form of **P** through a priori estimation. Most optimal interpolation schemes used in numerical weather prediction assume that the error field

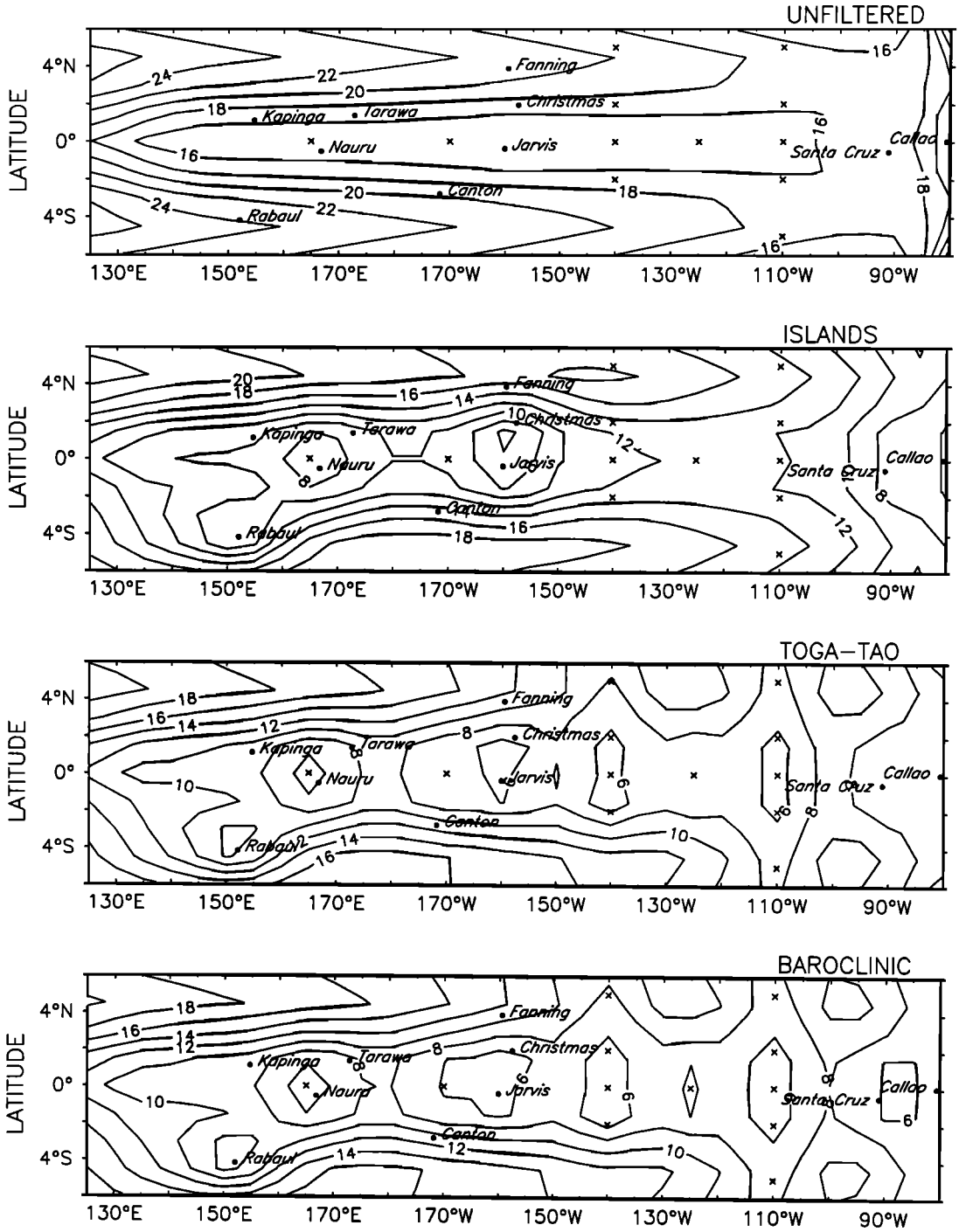

Fig. 11. Contour maps of expected rms error in 20° isotherm depth anomaly. Contour levels are in meters.

is spatially homogeneous, which it is not in the present case; see Figure 8 above and Figure 5*a* of MC. As noted in section 8c of MC, a homogeneous optimal interpolation scheme might be satisfactory far from boundaries, and a generalized scheme with spatially inhomogeneous error covariance could be easily constructed, given the Kalman filter results in hand, but it hardly seems worth the effort for this purpose. The reason to use optimal interpolation rather than the Kalman filter in any case is to save computing resources, and all of the computations that went into the present study required less than an hour on the Cray X/MP-48 at NCAR.

The error estimates obtained from the dynamical model were shown to converge to their steady values more slowly than expected. Even considering the first baroclinic mode Kelvin wave, the component which should equilibrate most rapidly, satisfactory convergence required six years of simulation. The variation of calculated statistics about their expected values from one realization to another proved to be much greater than initially expected, as shown in

TABLE 5. Statistics of 20° Isotherm Depth Anomaly Hindcast Experiments

Station	Location	Total Variance	Error Variances					
			ISL-REF[a]	EST[b]	TOGA-REF[c]	EST[d]	BARO-REF[e]	EST[f]
Kapinga	1.1N 155E	390(51)	104(20)	97	73(10)	78	75(12)	73
Tarawa	1.4N 173E	493(81)	72(9)	71	67(11)	54	58(11)	51
Canton	2.8S 172W	528(85)	270(53)	195	133(20)	105	137(24)	100
Fanning	3.9N 159W	643(81)	226(37)	242	144(30)	124	135(23)	120
TG2-1	2 N 141E	582(81)	148(31)	159	114(19)	133	121(18)	122
TG2-2	0 141E	335(40)	96(18)	95	81(14)	82	82(13)	75
TG2-3	5 N 155E	449(88)	325(59)	423	371(66)	320	300(54)	303
TG2-4	5 N 95 W	432(86)	119(24)	128	109(22)	113	95(18)	106

Variances are in square meters. Figures in parentheses are bootstrap standard deviations based on 200 bootstrap samples.

[a]Variance of the series of differences between the output of experiment ISL and the reference data set.

[b]The a priori estimate of the variance of ISL-REF generated by the Kalman filter.

[c]Variance of the series of differences between the output of experiment TOGA and the reference data set.

[d]The a priori estimate of the variance of TOGA-REF generated by the Kalman filter.

[e]Variance of the series of differences between the output of experiment BARO and the reference data set.

[f]The a priori estimate of the variance of BARO-REF generated by the Kalman filter.

Figure 1. This result should be a caution to interpretation of calculated statistics from short data series.

Statistics of the differences between the simulated data set and the output of the model driven by unperturbed winds compared well with statistical comparisons of model output with observed data. The bootstrap method was used to estimate the standard deviation of the sample variances, allowing judgment of whether the error variances relative to the simulated data and the error variances relative to the observed data were close to one another. In most cases, the variances fell within one standard deviation. The bootstrap method involves no specific assumption about the distribution of the errors. These statistics are the most persuasive evidence for the relevance of the simulation, and the ultimate justification for the use of the simple model.

Assimilation of sea level height data at the TOGA-TAO mooring locations resulted in considerable improvement. The estimated errors in that sea level height analysis were about 3 cm across most of the basin. This matches the accuracy of the monthly mean sea level anomaly data from the tide gauges, a rather impressive achievement. The data from the TOGA-TAO moorings contain information about the structure of the water column, and it was hoped that the details of that structure could be used to advantage. Assimilating the contributions of the two baroclinic modes separately made much less difference than initially expected; in fact, the improvement resulting from the inclusion of the extra detail was too small to be of any importance. It should be noted here that detailed assumptions were made about the observation errors. Changes in the error models could well change the results. However, the estimate used here of the accuracy of the separate modal contribution to dynamic height was almost certainly optimistic. Given this fact, the conclusion that the separate assimilation of the modes makes little difference is unlikely to be overturned.

The assumption made here that the statistics of the error field are spatially homogeneous is certainly questionable. The most simple-minded hypothesis, that the winds are best known where they have been sampled most often in a given month, leads to a highly inhomogeneous picture of the error; see, e.g., the map of the density of wind observations for March 1987 by *Reynolds et al.* [1989]. Comparisons between different wind products also show marked inhomogeneity [*Halpern and Harrison*, 1982; *Chelton and O'Brien*, 1982; *Harrison et al.*, 1989]. The question is, how much difference does this make in the analysis? Studies of the sensitivity of model results to parameterization of error statistics are planned.

The ultimate justification for the dynamical and statistical models used here is that these are the simplest models which will yield useful results. It should go without saying that there is no claim that the ocean is linear or homogeneous in vertical and lateral structure, or that no error results from making these assumptions which are known to be false to some degree. Similarly, no such extravagant claims are made for the simple statistical model of the errors. Order of magnitude estimates of errors arising from nonlinearity or spatially nonuniform wave propagation speed indicate that such errors are small compared to errors arising from 2 m/s errors in the wind field. The results presented here indicate that adding synthetic errors of that magnitude to a standard wind product results in errors in the sea level height fields which are, in most cases, statistically indistinguishable from the errors found in comparisons with real data. Interpretation of differences in results which might follow from more detailed dynamical or statistical models would therefore be questionable.

The results of this work, along with those in MC are consistent with the view that the dynamical model used here, however simple, is as detailed a model as the data will support. Even so, it depends on an expansion in meridional modes which, because of its convergence characteristics, limits the region of validity of the model to a small range of latitudes near the equator. The production of useful maps and the computation of initial values for practical forecast models such as that of *Zebiak and Cane* [1987] require a model valid over a greater extent. An example of such a model is that of *Cane and Patton* [1984]. Extension of these results to that model is planned.

In MC, only sea level height was considered for analysis and assimilation. In the present work, analyzed fields of the 20° isotherm were produced with results comparable to those obtained in the sea level experiments. Such fields are suitable for studies incorporating hydrographic data such as the TOGA XBT's.

Acknowledgments. The author would like to thank Mark Cane and Stanley P. Hayes for helpful discussions and critical reading of early drafts of this manuscript, and Robert Myers for assistance in all aspects of computing. This work was supported by the National Science Foundation grant OCE86-11434. Major computations were performed on the Cray X/MP-48 at NCAR. The National Center for Atmospheric Research is supported by the National Science Foundation.

REFERENCES

Bennett, A. F., and W. P. Budgell, The Kalman smoother for a linear quasi-geostrophic model of ocean circulation, *Dyn. Atmos. Oceans*, *13*, 219–267, 1989.

Busalacchi, A. J., and M. A. Cane, The effect of varying stratification on low-frequency equatorial motions, *J. Phys. Oceanogr.*, *18*, 801–812, 1988.

Cane, M. A., Modeling sea level during El Niño, *J. Phys. Oceanogr.*, *14*, 1864–1874, 1984.

Cane, M. A., and A. J. Busalacchi, Atlantic Seasonality, III, Conclusions, in *Further Progress in Equatorial Oceanography*, edited by E. Katz and J. Witte, pp. 255–258, Nova University Press, Ft. Lauderdale, Fla., 1987.

Cane, M. A., and R. J. Patton, A numerical model for low-frequency equatorial dynamics, *J. Phys. Oceanogr.*, *14*, 586–606, 1984.

Cane, M. A., and E. S. Sarachik, Forced baroclinic ocean motions, II, The linear equatorial bounded case, *J. Mar. Res.*, **35**, 395–432, 1977.

Chelton, D. B., and J. J. O'Brien, Satellite microwave measurements of surface wind speed in the tropical Pacific, *Trop. Ocean Atmos. Newslett.*, *11*, 2–4, 1982.

Efron, B., and G. Gong, A leisurely look at the bootstrap, the jackknife, and cross-validation, *Am. Stat.*, *37*, 36–48, 1983.

Gelb, A. (ed.), *Applied Optimal Estimation*, 374 pp., MIT Press, Cambridge, Mass., 1974.

Ghil, M., S. E. Cohn, J. Tavantzis, K. Bube, and E. Isaacson, Applications of estimation theory to numerical weather prediction, in *Dynamic Meteorology: Data Assimilation Methods, Appl. Math. Sci. Ser.*, vol. 36, edited by L. Bengtsson, et al., pp. 139–224, Springer-Verlag, New York, 1981.

Goldenberg, S. B., and J. J. O'Brien, Time and space variability of tropical Pacific wind stress, *Mon. Weather Rev.*, *109*, 1190–1207, 1981.

Halpern, D., On the accuracy of monthly wind speeds over the equatorial Pacific, *J. Atmos. Oceanic Technol.*, *5*, 362–367, 1988.

Halpern, D., and D. E. Harrison, Intercomparison of tropical Pacific mean November 1979 surface wind fields, *Rep. 82-1*, 40 pp., Dep. of Meteorol. and Phys. Oceanogr., Mass. Inst. of Technol., Cambridge, 1982.

Harrison, D. E., W. S. Kessler, and B. J. Giese, Ocean circulation and model hindcasts of the 1982-82 El Niño: Thermal variability along the ship-of-opportunity tracks, *J. Phys. Oceanogr.*, *19*, 397–418, 1989.

Hayes, S.P., The Atlas wind and thermal structure array, in US TOGA Ocean Observation System Mid-life Progress Review and Recommendations for Continuation, Workshop Rep., pp. C46–C48, Nova University Press, Ft. Lauderdale, Fla., 1989.

Hayes, S. P., P. Ripa, and L. J. Mangum, On resolving vertical modes with observational data, *J. Geophys. Res.*, *90*, 7227–7234, 1985.

Hayes, S. P., M. J. McPhaden, and A. Leetmaa, Observational verification of a quasi real time simulation of the tropical Pacific ocean, *J. Geophys. Res.*, *94*, 2147–2157, 1989.

Long, R. B., and W. C. Thacker, Data assimilation into a numerical equatorial ocean model, II, Assimilation experiments, *Dyn. Atmos. Oceans*, *13*, 413–439, 1989.

McPhaden, M. J., J. A. Proehl, and L. M. Rothstein, The interaction of equatorial Kelvin waves with realistically sheared zonal currents, *J. Phys. Oceanogr.*, *16*, 1499–1515, 1986.

Miller, R. N., Toward the application of the Kalman filter to regional open ocean modeling, *J. Phys. Oceanogr.*, *16*, 72–86, 1986.

Miller, R. N., and M.A. Cane, A Kalman filter analysis of sea level height in the tropical Pacific, *J. Phys. Oceanogr.*, *19*, 773–790, 1989.

Rebert, J. P., J. R. Donguy, G. Eldin, and K. Wyrtki, Relations between sea level, thermocline depth, heat content and dynamic height in the tropical Pacific ocean, *J. Geophys. Res.*, *90*, 11,719–11,725, 1985.

Reynolds, R. W., K. Arpe, C. Gordon, S. P. Hayes, A. Leetmaa, and M. J. McPhaden, A comparison of tropical Pacific surface wind analyses, *J. Clim.*, *2*, 105–111, 1989.

Schlatter, T. W., G. W. Branstator, and L. G. Thiel, Testing a global multivariate statistical objective analysis scheme with observed data, *Mon. Weather Rev.*, *104*, 765–783, 1976.

Weisberg, R. H., Observations pertinent to instability waves in the equatorial oceans, in *Further Progress in Equatorial Oceanography*, edited by E. Katz and J. Witte, pp. 335–350, Nova University Press, Ft. Lauderdale, Fla., 1987.

Zebiak, S.E., and M.A. Cane, A model El Niño southern oscillation, *Mon. Weather Rev.*, *115*, 2262–2278, 1987.

R. N. Miller, College of Oceanography, Oregon State University, Oceanography Admin. Bldg. 104, Corvallis, OR 97331-5503.

(Received October 2, 1989;
revised February 15, 1990;
accepted March 6, 1990.)